Molecular Cell

Article

# BUB1 and CENP-U, Primed by CDK1, Are the Main PLK1 Kinetochore Receptors in Mitosis

## Graphical Abstract

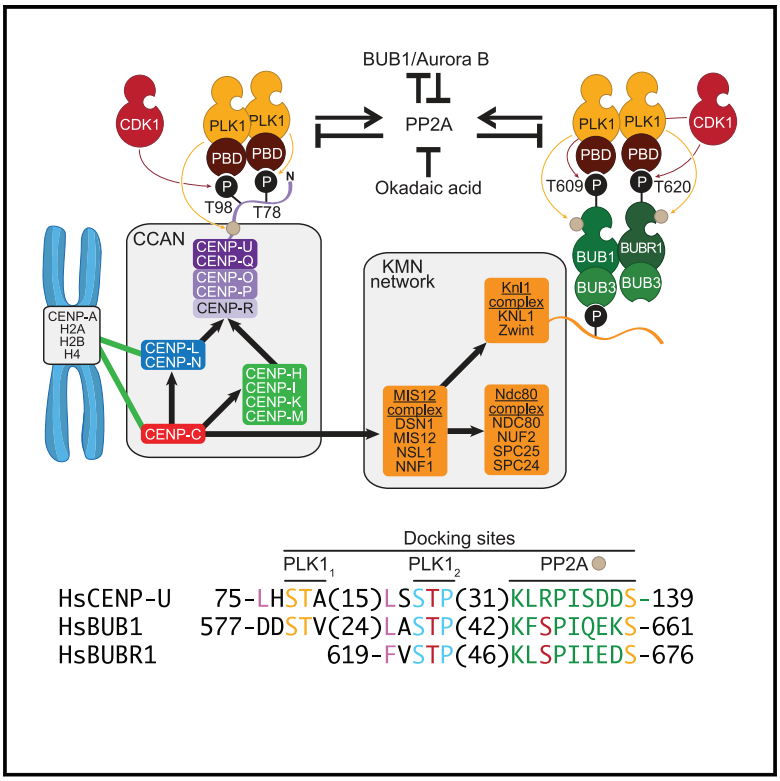


## Highlights

- Recruitment of PLK1 to BUB1 and to the core kinetochore is reconstituted *in vitro*
- The CENP-U N-terminal region exposes the only PLK1 receptor in the core kinetochore
- CDK1 and PLK1 promote PLK1 recruitment on BUB1 and CENP-U and PLK1 dimerization
- Like BUB1, CENP-U contains a previously unnoticed PP2A-phosphatase-binding motifs


## Authors

Priyanka Singh, Marion E. Pesenti, Stefano Maffini, ..., Anupallavi Srinivasamani, Tanja Bange, Andrea Musacchio

## Correspondence

andrea.musacchio@mpi-dortmund.mpg.de



## In Brief

Polo-like kinase 1 (PLK1) targets kinetochores to regulate microtubule attachment and mitotic checkpoint signaling. Singh et al. show how CDK1 and PLK1 promote kinetochore recruitment and dimerization of PLK1 onto BUB1 and CENP-U, probably the only PLK1 receptors in the core kinetochore. A conserved constellation of docking sites in BUB1 and CENP-U, including one for PP2A phosphatase, suggests a common regulatory switch.


Singh et al., 2021, Molecular Cell *81*, 67–87
January 7, 2021 
https://doi.org/10.1016/j.molcel.2020.10.040

CellPress

Molecular Cell

CellPress
OPEN ACCESS

Article

# BUB1 and CENP-U, Primed by CDK1, Are the Main PLK1 Kinetochore Receptors in Mitosis

Priyanka Singh,[1,3,7] Marion E. Pesenti,[1,7] Stefano Maffini,[1] Sara Carmignani,[1] Marius Hedtfeld,[1] Arsen Petrovic,[1,4] Anupallavi Srinivasamani,[1,5] Tanja Bange,[1,6] and Andrea Musacchio[1,2,8,*]

[1]Department of Mechanistic Cell Biology, Max Planck Institute of Molecular Physiology, Otto-Hahn-Straße 11, 44227 Dortmund, Germany
[2]Centre for Medical Biotechnology, Faculty of Biology, University Duisburg-Essen, Universitätsstrasse, 45141 Essen, Germany
[3]Present address: Department of Bioscience & Bioengineering, Indian Institute of Technology Jodhpur, NH65, Nagaur Road, Karwar 342037, Jodhpur, Rajasthan, India
[4]Present address: Department of Molecular Structural Biology, Max Planck Institute of Biochemistry, Am Klopferspitz 18, 82152 Martinsried, Germany
[5]Present address: Department of Immunology, University of Texas MD Anderson Cancer Center, 1515 Holcombe Boulevard, Unit 901, Houston, TX 77054, USA
[6]Present address: Department for Systems Chronobiology, Institute of Medical Psychology, LMU Munich, Goethe-Str. 31, 80336 Munich, Germany
[7]These authors contributed equally
[8]Lead Contact
*Correspondence: andrea.musacchio@mpi-dortmund.mpg.de
https://doi.org/10.1016/j.molcel.2020.10.040

## SUMMARY

Reflecting its pleiotropic functions, Polo-like kinase 1 (PLK1) localizes to various sub-cellular structures during mitosis. At kinetochores, PLK1 contributes to microtubule attachments and mitotic checkpoint signaling. Previous studies identified a wealth of potential PLK1 receptors at kinetochores, as well as requirements for various mitotic kinases, including BUB1, Aurora B, and PLK1 itself. Here, we combine ectopic localization, *in vitro* reconstitution, and kinetochore localization studies to demonstrate that most and likely all of the PLK1 is recruited through BUB1 in the outer kinetochore and centromeric protein U (CENP-U) in the inner kinetochore. BUB1 and CENP-U share a constellation of sequence motifs consisting of a putative PP2A-docking motif and two neighboring PLK1-docking sites, which, contingent on priming phosphorylation by cyclin-dependent kinase 1 and PLK1 itself, bind PLK1 and promote its dimerization. Our results rationalize previous observations and describe a unifying mechanism for recruitment of PLK1 to human kinetochores.

## INTRODUCTION

By catalyzing the post-translation phosphorylation of consensus motifs on their targets, protein kinases regulate, in space and time, countless biological processes (Ubersax and Ferrell, 2007). In the cell division cycle of eukaryotes, which ultimately results in cell duplication, several protein kinases have essential regulatory roles (Novak et al., 2010). In single-celled eukaryotes, including for *Saccharomyces cerevisiae* and *Schizosaccharomyces pombe*, a single member of the cyclin-dependent kinase family (CDK) is the "engine" of cell division. Progressive, controlled activation of this CDK orders in time the duplication of chromosomes during the S phase and their segregation during mitosis (Novak et al., 2010). This general scheme is conserved in multicellular eukaryotes, where additional CDKs with partly redundant functions exist (Novak et al., 2010).

Although CDK activity directs the cell cycle, it also regulates the activation of various other protein kinases that execute the multitude of events required for cell division (Saurin, 2018). Among them, Polo-like kinases represent a conserved family of effector kinases that orchestrate key functions in mitosis and cytokinesis (Archambault and Glover, 2009; Combes et al., 2017; Zitouni et al., 2014). Genes encoding members of this kinase family, *cdc5* and *polo*, were first identified in genetic screens in *S. cerevisiae* and *Drosophila melanogaster*, respectively (Hartwell et al., 1973; Llamazares et al., 1991; Sunkel and Glover, 1988). Polo orthologs were later identified in *S. pombe*, *Xenopus laevis*, and mammals, where they were named, respectively, Plo1, Plx1, and PLK1 (Clay et al., 1993; Golsteyn et al., 1994; Holtrich et al., 1994; Kumagai and Dunphy, 1996; Mulvihill et al., 1999; Ohkura et al., 1995). A requirement for Polo in mitotic progression and bipolar spindle formation was first identified in flies (Llamazares et al., 1991; Sunkel and Glover, 1988). In humans, PLK1 peaks between the G2 and M phases of the cell cycle, when PLK1 occupies sub-cellular locations that include centrosomes, kinetochores, microtubules, the central spindle, and the midbody (Ahonen et al., 2005; Arnaud et al., 1998; De Luca et al., 2006; Golsteyn et al., 1994, 1995; Goto et al., 2006; Lane

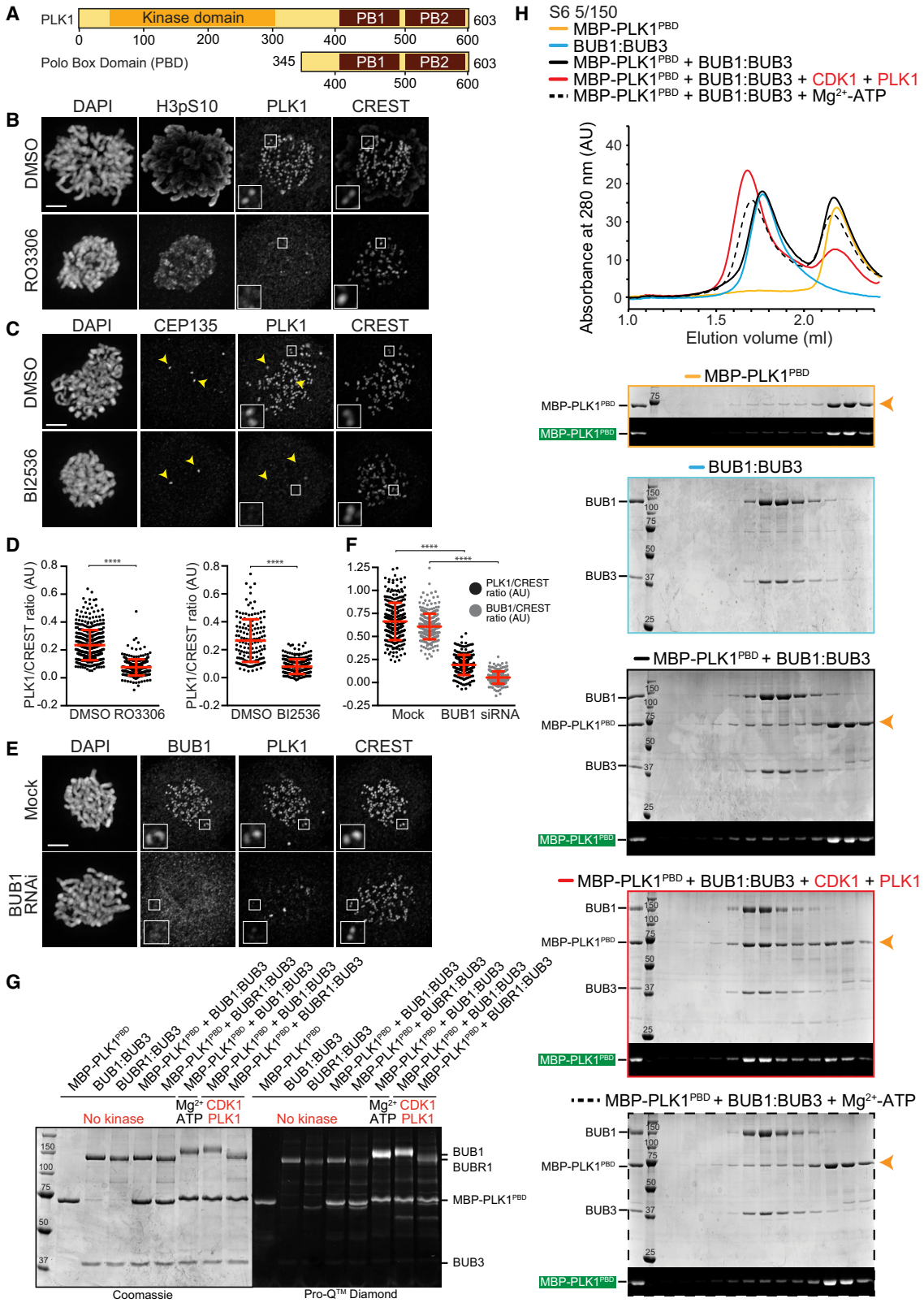


(legend on next page)

and Nigg, 1996; Lénárt et al., 2007; Liu et al., 2004; Neef et al., 2003). At these locations, PLK1 participates in functions that include mitotic entry, centrosome separation and maturation, chromosome alignment, spindle checkpoint signaling, and cytokinesis (Combes et al., 2017; Saurin, 2018).

PLK1 has an N-terminal catalytic Ser/Thr kinase domain and a C-terminal Polo-box domain (PBD; Figure 1A). The kinase domain phosphorylates target proteins on Ser or Thr within the consensus motif [**D**/**N**/**E**/Y]-X-S/T-[**F**/Φ; no P]-[Φ/X], where Φ and X indicate hydrophobic and any amino acid, respectively, and residues in bold indicate strong preference (Alexander et al., 2011; Dou et al., 2011; Hegemann et al., 2011; Heinrich et al., 2013; Kettenbach et al., 2011; Nakajima et al., 2003). The PBD (comprising residues 345–603 in human PLK1) includes two polo box (PB) motifs (residues 411–489 and 511–592), intervening residues, and part of the linker between the kinase domain and PB1 (residues 373–410) (Cheng et al., 2003; Elia et al., 2003b). The PBD mediates PLK1 localization and activation (Elia et al., 2003b; Hanisch et al., 2006; Jang et al., 2002a; Lee et al., 1998; Lowery et al., 2007; Seong et al., 2002). It docks onto a motif of binding partners characterized by the sequence Ser-[pSer/pThr]-[Pro/X], where pSer and pThr indicate phosphorylated serine and threonine, respectively, and X can be any residue (Elia et al., 2003a, 2003b). When X is proline (Pro), the PBD-binding motif embeds the core phosphorylation target of proline-directed kinases, such as CDK1, the main mitotic kinase, which target Ser/Thr-Pro motifs. Thus, CDK1 phosphorylation of these motifs generates binding sites for PLK1 (Elowe et al., 2007; Lowery et al., 2007; Moshe et al., 2004; Watanabe et al., 2004; Wong and Fang, 2007; Xu et al., 2013; Yamaguchi et al., 2005; Yamashiro et al., 2008; Yoo et al., 2004). In addition, the PBD may interact with non-phosphorylated motifs or with motifs phosphorylated by PLK1 itself (self-priming). Self-priming may become especially relevant after the decline of CDK activity at anaphase (Burkard et al., 2009; García-Alvarez et al., 2007; Kang et al., 2006; Lee et al., 2014; McKinley and Cheeseman, 2014; Neef et al., 2003, 2007; Park et al., 2010; Wolfe et al., 2009). Collectively, these interactions mediate the recruitment of PLK1 to various subcellular locations (Archambault and Glover, 2009; Combes et al., 2017; Zitouni et al., 2014) and, in addition, contribute to stimulate its kinase activity by relieving an intra-molecular interaction of the PBD and kinase domain that stabilizes an inactive conformation of PLK1 (Mundt et al., 1997; Xu et al., 2013). Activation of PLK1 also requires phosphorylation by Aurora A or Aurora B, related kinases localizing, respectively, at spindle poles and centromeres-kinetochores on Thr210 of the PLK1 activation loop (Carmena et al., 2012; Jang et al., 2002b; Johnson et al., 2008; Kelm et al., 2002; Kothe et al., 2007; Macůrek et al., 2008; Seki et al., 2008; Xu et al., 2013).

Centromeres are chromosome *loci* that provide a foundation for the kinetochore, a multi-subunit complex whose primary function is the capture, through specialized machinery that includes the NDC80 complex (Cheeseman et al., 2006; DeLuca et al., 2006; Pesenti et al., 2018). Microtubule binding to kinetochores is necessary but not sufficient for chromosome bi-orientation and segregation. The latter requires a local, kinetochore- and centromere-confined regulatory network of several mitotic kinases, including CDK1, Aurora B, BUB1, MPS1, PLK1, their many substrates, and counteracting protein phosphatases, including PP1 and PP2A (Saurin, 2018). Treatments that interfere with these regulators expose dramatic defects in chromosome alignment. The network modulates the stability of kinetochore-microtubule attachments, most notably, but not exclusively, through multisite phosphorylation of NDC80 (Monda and Cheeseman, 2018; Musacchio and Desai, 2017) and is thought to respond to different levels of microtubule-generated forces on mono-oriented (and incorrectly oriented) or bi-oriented chromosomes, respectively (Nezi and Musacchio, 2009; Rago and Cheeseman, 2013). How the force-sensing mechanism operates is obscure, but Aurora B and PLK1 appear to oppose each other, acting, respectively, to destabilize and stabilize the kinetochore-microtubule interface (Foley et al., 2011; Liu et al., 2012).

Studying bi-orientation and its feedback control is enormously challenging, not least because it is accomplished within the very restricted volume of the kinetochore-centromere region, whose

**Figure 1. BUB1 Is a Prominent Kinetochore Receptor of PLK1**

(A) Scheme of human PLK1.

(B) HeLa cells were released from double-thymidine block into nocodazole (3.3 μM) to synchronize in prometaphase. Cells were exposed to DMSO or RO3306 for 10 min in the presence of MG132 before fixation. Representative cells for DMSO and RO3306 were immunostained for DAPI (DNA marker), H3pS10 (Aurora B activity marker), PLK1, and CREST (kinetochore marker). Intensities from 436 kinetochores for DMSO-treated cells and 289 for RO3306 in five to six cells were scored. Scale bar, 5 μm.

(C) HeLa cells, synchronized as in (B), were exposed to DMSO or BI2536 for 90 min in the presence of MG132 before fixation. Cells were immunostained for DAPI, CEP135 (centrosome marker), PLK1, and CREST. Yellow arrowheads highlight centrosomes. Intensities from 143 kinetochore for DMSO-treated and 291 for BI-2536 treatment in four to five cells were scored.

(D) Dot plots representing PLK1/CREST intensity ratios for individual kinetochores. Statistical significance in all figures reflects Mann-Whitney test (see Method Details). Error bars represent means ± standard errors of the mean.

(E) Representative images showing mock and BUB1-depleted HeLa cell immunostained for DAPI, BUB1, PLK1, and CREST.

(F) Dot plots representing PLK1/CREST kinetochore intensity ratio (black bars) and mean BUB1/CREST kinetochore ratio (gray bars) in the case of BUB1 RNAi. Error bars represent means ± standard errors of the mean; 303 kinetochores for mock and 232 kinetochores for BUB1 RNAi in four to five different cells were scored.

(G) Phosphorylation of input proteins of SEC experiment in (H) and Figure S3B were assessed by SDS-PAGE, followed by Coomassie or Pro-Q Diamond staining. The same gels are also displayed in Figure S2A.

(H) Elution profile and SDS-PAGE analysis of an SEC run on a Superose6 5/150 column (S6 5/150) of the interaction of Alexa-488-labeled MBP-PLK1$^{PBD}$ with the BUB1:BUB3 complex (5 μM each) in the presence of the indicated priming kinases (marked in red; used at 1/20 ratio). In-gel fluorescence of Alexa-488-labeled MBP-PLK1$^{PBD}$ in the SEC fractions analyzed by SDS-PAGE is also shown. The orange arrows highlight MBP-PLK1$^{PBD}$ in each gel. The MBP-PLK1$^{PDB}$ control elution profile and SDS-PAGE are also displayed in Figure S3A.

nanoscale organization is incompletely understood. Specific sub-localizations of the regulators within this restricted volume establish short-range (tens or hundreds of nanometer) and dynamic spatial activity gradients that are likely to be crucial for the tension-sensing mechanism (Krenn and Musacchio, 2015; Lampson and Grishchuk, 2017). Before mechanistic insight into these dynamics can be gained, how and where, in kinetochores, the different mitotic kinases and phosphatases are recruited must be understood. Here, we elucidate kinetochore recruitment of PLK1 in mitotic human cells. Previous work suggested that this recruitment depends on a remarkably long list of docking partners, including BUB1 and its paralog BUBR1, CLASP2, INCENP, and survivin (subunits of the Aurora-B-containing chromosome passenger complex [CPC]), SGO1 (a CPC-, PP2A-, and cohesin-associated protein), dynactin, NUDC (a regulator of dynein and LIS1), CLIP 170 (a microtubule-binding protein), NCAPG2 (a condensin subunit), Meikin (a meiotic protein), RSF1 (a chromatin remodeler), CENP-U (also named CENP-50 or PBIP1, an inner kinetochore protein), and USP16 (a deubiquitinase) (Amin et al., 2014; Goto et al., 2006; Ikeda and Tanaka, 2017; Kang et al., 2006, 2011; Kim et al., 2014, 2015; Lee et al., 2015; Maia et al., 2012; Matsumura et al., 2007; Nishino et al., 2006; Pouwels et al., 2007; Qi et al., 2006; Sun et al., 2012; Yeh et al., 2013; Zhuo et al., 2015). It is unclear whether these proteins, individually, are bona fide receptors of PLK1 or are, rather, part of a hierarchical regulatory network that eventually converges on PLK1 recruitment to only one or a few of them. In favor of the latter, although the receptors listed above are scattered through the entire centromere and kinetochore, PLK1 occupies a smaller, focused region of the kinetochore (Lénárt et al., 2007; Lera et al., 2016), suggesting a specific interaction with one or a few confined receptors. Even within this confined localization, regulation of PLK1 binding may be complex. For instance, although a role of CDK1 in the recruitment of PLK1 to BUB1 and BUBR1 is well established, PLK1 has also been proposed to bind CENP-U in mitosis simply through self-priming (Kang et al., 2006, 2011).

Here, we demonstrate physical interactions of PLK1 with BUB1, BUBR1, and CENP-U and show that CENP-U may be the sole, prominent PLK1 receptor within the kinetochore core. Aurora B and BUB1 promote PLK1 binding to CENP-U, but their requirement is indirect and can be bypassed. Importantly, binding of PLK1 to CENP-U is strictly dependent on priming CDK1 activity, which promotes robust PLK1 docking through PLK1 dimerization on Thr78 (T78), previously identified as the PLK1 self-priming site (Kang et al., 2006, 2011), and Thr98. A conserved and unique constellation of binding motifs in BUB1, BUBR1, and CENP-U suggests a unifying view of the PLK1 kinetochore recruitment mechanism.

## RESULTS

### Role of PLK1, CDK1, and BUB1 in Kinetochore Recruitment of PLK1

PLK1 interacts with binding partners through self-priming or through CDK1 priming activity (Lowery et al., 2005). To test whether PLK1 or CDK1 promote kinetochore recruitment of PLK1 in HeLa cells, we individually inhibited them in mitotically arrested cells (nocodazole, 3.3 μM) with highly selective small-molecule inhibitors of PLK1 (BI2536, used at 100 nM) or CDK1 (RO3306, 9 μM) (Lénárt et al., 2007; Vassilev et al., 2006) and analyzed kinetochore localization at 10, 30, and 90 min in the presence of the proteasome inhibitor MG132 (10 μM) to prevent mitotic exit (Figures S1A–S1G). Both inhibitors caused a very prominent reduction of kinetochore PLK1, as assessed by immunofluorescence (Figures 1B–1D). BI2536 depleted PLK1 not only from kinetochores but also from mitotic centrosomes, as described (Lénárt et al., 2007).

Kinetochore recruitment of PLK1 requires at least two additional kinases, BUB1 and Aurora B (subunit of the CPC) (Goto et al., 2006; Qi et al., 2006; Sun et al., 2012). Indeed, depletion of BUB1 by small interfering RNA (siRNA) interference (Figure S1H; validated by disappearance of the H2A-pT120 mark in Figure S1I) largely depleted PLK1 from kinetochores (Figures 1E and 1F). Thus, recruitment of PLK1 to kinetochores requires the kinase activity of CDK1 and PLK1 and at least the presence of BUB1. Phosphorylation of BUB1 and BUBR1 by CDK1 kinase, respectively, on Thr609 and Thr620, which lie within Ser-Thr-Pro (STP) motifs, preludes PLK1 recruitment (Elowe et al., 2007; Huang et al., 2008; Qi et al., 2006; Wong and Fang, 2007). In kinase assays *in vitro*, recombinant BUB1:BUB3 incubated with $Mg^{2+}$-ATP only strongly auto-phosphorylated, as revealed by shifts in the electrophoretic mobility in SDS-PAGE and staining of phosphorylated proteins with Pro-Q Diamond (Figures 1G and S2A). BUB1 became even more strongly phosphorylated in the presence of sub-stoichiometric concentrations of priming CDK1 and PLK1 (in this and other experiments, priming kinases were used at 1/10 to 1/30 ratio to their substrate; in figures, priming kinases are marked in red). BUBR1:BUB3, which does not auto-phosphorylate (unpublished data; Breit et al., 2015; Suijkerbuijk et al., 2012a), also became phosphorylated with priming CDK1 and PLK1, albeit less than BUB1:BUB3 (Figures 1G and S2A).

Next, we combined primed BUB1:BUB3 or BUBR1:BUB3 with a fluorescently labeled fusion of maltose-binding protein (MBP) and the PLK1 Polo-box domain (MBP-PLK1$^{PBD}$; Figure 1A), which is sufficient for kinetochore targeting. To detect binding, the mix was analyzed by size-exclusion chromatography (SEC). Both BUB1:BUB3 and BUBR1:BUB3 formed stoichiometric complexes with Alexa-488-labeled MBP-PLK1$^{PBD}$, but only after treatment with priming CDK1 and PLK1 (Figures 1H and S3A). Without priming kinases, addition of $Mg^{2+}$-ATP did not promote binding to MBP-PLK1$^{PBD}$, indicating that despite considerable auto-phosphorylation BUB1 kinase activity is not required for binding to MBP-PLK1$^{PBD}$. These observations are in line with previous work on the role of BUB1 and BUBR1 as PLK1 receptors (Cordeiro et al., 2020; Elowe et al., 2007; Qi et al., 2006) and show that CDK1 and PLK1 prime BUB1 and BUBR1 to become direct binding partners of PLK1$^{PBD}$.

### Aurora B and BUB1 Contribute Indirectly to PLK1 Recruitment

MPS1 phosphorylates KNL1 to generate binding sites for BUB1 (and, indirectly, through the latter for BUBR1) (Krenn et al., 2014; Overlack et al., 2015; Vleugel et al., 2013). In agreement with those previous studies, inhibition of MPS1 with Reversine

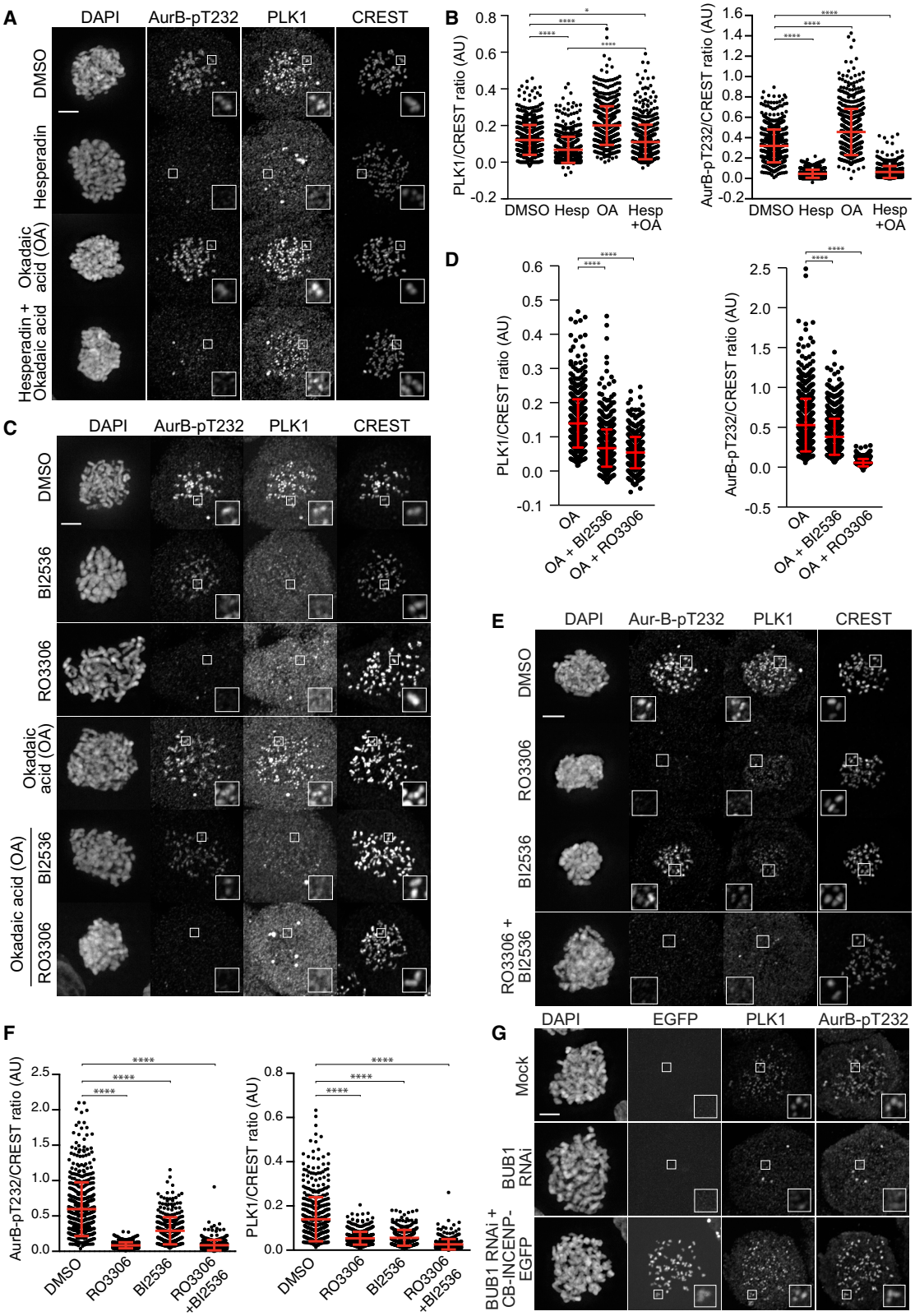


*(legend on next page)*

(Santaguida et al., 2010) led to a strong decrease of BUB1 kinetochore levels (Figures S4A and S4B), concomitant with the previously reported increase of MPS1 kinetochore levels (Santaguida et al., 2010) (Figures S4C and S4D). The kinetochore levels of PLK1 correlated with those of BUB1, with reduced but residual kinetochore localization (Figures S4E and S4F).

Next, we tested a requirement for Aurora B in PLK1 kinetochore recruitment. The selective Aurora B inhibitor hesperadin (500 nM) (Hauf et al., 2003) ablated H3-pS10 (phosphorylated Ser10 of Histone H3, a mitotic substrate of Aurora B [Hsu et al., 2000]). PLK1 levels were significantly reduced in comparison to DMSO-treated control cells, indicating that Aurora B is also required for kinetochore recruitment of PLK1 (Figures S2B and S2C). Aurora B may control PLK1 recruitment in various ways. First, Aurora B is required for kinetochore recruitment of BUB1 (Morrow et al., 2005), which, in turn, recruits PLK1. Second, Aurora B exercises homeostatic control of the levels of kinetochore phosphorylation by controlling the major human mitotic phosphatases PP1 and PP2A (reviewed in Joukov and De Nicolo, 2018, and Saurin, 2018). Interference with Aurora B activity might, therefore, cause ectopic activation of phosphatases that counteract PLK1 kinetochore recruitment through hydrolysis of phosphosites required for PLK1 docking. Third, Aurora B phosphorylates the activation loop of PLK1, activating it (Carmena et al., 2012; Shao et al., 2015).

To dissect these complex interdependencies, we focused on PP1 and PP2A, both of which are inhibited by okadaic acid (OA) (Bialojan and Takai, 1988). We treated mitotic HeLa cells with hesperadin, OA (100 nM), or their combination in nocodazole and MG132. After 90 min, cells were fixed and processed for immunofluorescence. In isolation, OA caused a marked increase of kinetochore PLK1 and AurB-pT232 (an Aurora B auto-phosphorylation site (Sessa et al., 2005)). OA also rescued the detrimental effects of Aurora B inhibition, allowing kinetochore accumulation of PLK1 in hesperadin-treated cells to levels almost comparable to those in DMSO-treated cells (Figures 2A and 2B). This was not due to re-activation of Aurora B because the levels of AurB-pT232 remained low (Figures 2A and 2B). Similarly, and in agreement with previous studies (De Antoni et al., 2012), Aurora B kinetochore levels were not affected by hesperadin, OA, or their combination (Figures S4G and S4H). Thus, PLK1 can be recruited to kinetochores when Aurora B is inhibited, if the phosphatase activity is also suppressed. This suggests that Aurora B is not directly required for PLK1 kinetochore recruitment. Rather, its requirement may reflect regulation of phosphatases that control the abundance of phospho-epitopes directly or indirectly involved in PLK1 recruitment.

We addressed the role of CDK1 and PLK1 using the same assay. As already shown (Figures 1B–1D), BI2536 or RO3306 strongly counteracted kinetochore recruitment of PLK1 (Figures 2C, 2D, and S1A–S1F). In addition, RO3306 strongly inhibited the accumulation of AurB-pT232, probably because CDK1 activity is required for efficient CPC recruitment to centromeres and kinetochores (Krenn and Musacchio, 2015). Importantly, OA did not promote re-accumulation of PLK1 at kinetochores in the presence of BI2536 or RO3306, suggesting that the activity of both CDK1 and PLK1 is directly required for PLK1 kinetochore recruitment (Figures 2C, 2D, and S1J). Indeed, PLK1 almost disappeared from mitotic kinetochores in HeLa cells co-treated with BI2536 or RO3306 (Figures 2E and 2F).

## Another Kinetochore Binding Site for PLK1

BUB1 is required for kinetochore localization of BUBR1 (Overlack et al., 2015), possibly explaining why BUBR1 depletion has no major consequences on kinetochore PLK1 (Cordeiro et al., 2020; Elowe et al., 2007). BUB1 also contributes to a positive feedback loop that promotes localized accumulation and activation of Aurora B (Baron et al., 2016; Caldas et al., 2013; Hindriksen et al., 2017; Liu et al., 2013; van der Waal et al., 2012; Wang et al., 2011). Indeed, depletion of BUB1 by RNAi prevented accumulation of the active form of Aurora B (Figure 2G, middle). This raises a conundrum because it implies that depletion of BUB1, in addition to removing binding sites for PLK1 on BUB1 and BUBR1, may also interfere with other Aurora-B-dependent interactions of PLK1, even if only indirectly through control of protein phosphatases. To test that, we resorted to a CENP-B-INCENP-EGFP chimera (CB-INCENP-EGFP; Figure S2D) (Liu et al., 2009), in which the centromere-targeting domain of CB is fused to INCENP, a CPC subunit required for Aurora B localization and activation (Adams et al., 2000; Kaitna et al., 2000). Expression of CB-INCENP-EGFP in BUB1-depleted cells largely restored the levels of AurB-pT232 (Figures S2E–S2G). Remarkably, it also promoted kinetochore localization of PLK1 to levels almost comparable to control cells (Figures 2G, bottom, S2F, and S2G), revealing that another kinetochore receptor for PLK1 must exist, in addition to BUB1 and BUBR1.

**Figure 2. PLK1 and CDK1 Activity Is Required for Kinetochore Recruitment of PLK1**

(A) Representative images of pro-metaphase-synchronized HeLa cells treated with DMSO, hesperadin (500 nM, here and elsewhere), okadaic acid (100 nM, here and elsewhere), or hesperadin plus okadaic acid for 90 min with MG132. Cells were immunostained for DAPI, Aur-pT232, PLK1, and CREST.

(B) Dot plots of PLK1/CREST (left) or AurB-pT232/CREST (right) intensity ratio for individual kinetochores; 734 kinetochores for DMSO, 689 for hesperadin, 684 for okadaic acid and 650 for hesperadin + okadaic acid-treated cells in eight to 12 different cells were scored. Error bars, means ± standard errors of the mean.

(C) Representative pro-metaphase-synchronized HeLa cells treated with DMSO, BI 2536, RO3306, okadaic acid, and RO3306 or BI 2536 plus okadaic acid for 90 min (10 min in the case of RO3306) in the presence of MG132. Cells were immunostained for DAPI, AurB-pT232, PLK1, and CREST. Scale bar, 5 μm.

(D) Dot plots representing PLK1/CREST (left) and AurB-pT232 over CREST (right) intensity ratios for individual kinetochores; 382 to 1,298 individual kinetochores in seven to 17 different cells were scored. The red line indicates means ± standard deviation. Additional controls in Figure S1J.

(E) Representative images of prometaphase synchronized HeLa cells treated with DMSO (control), RO3306, BI2536, or RO3306 + BI2536, stained with DAPI, AurB-pT232, PLK1, and CREST. Scale bar, 5 μm.

(F) Dot plots of AurB-pT232/CREST (left) or PLK1/CREST (right) intensity ratios for individual kinetochores. Error bars represent means ± standard errors of the mean; 426–541 individual kinetochores in seven to 11 different cells were scored.

(G) Representative images showing mock, BUB1-RNAi alone, or concomitantly expressing doxycycline-inducible CB-INCENP-EGFP in HeLa cells. Cells were immunostained for DAPI, PLK1, and phosphorylated T232 residue of Aurora B (AurB-pT232). EGFP reflects CB-INCENP expression. Scale bar, 5 μm.

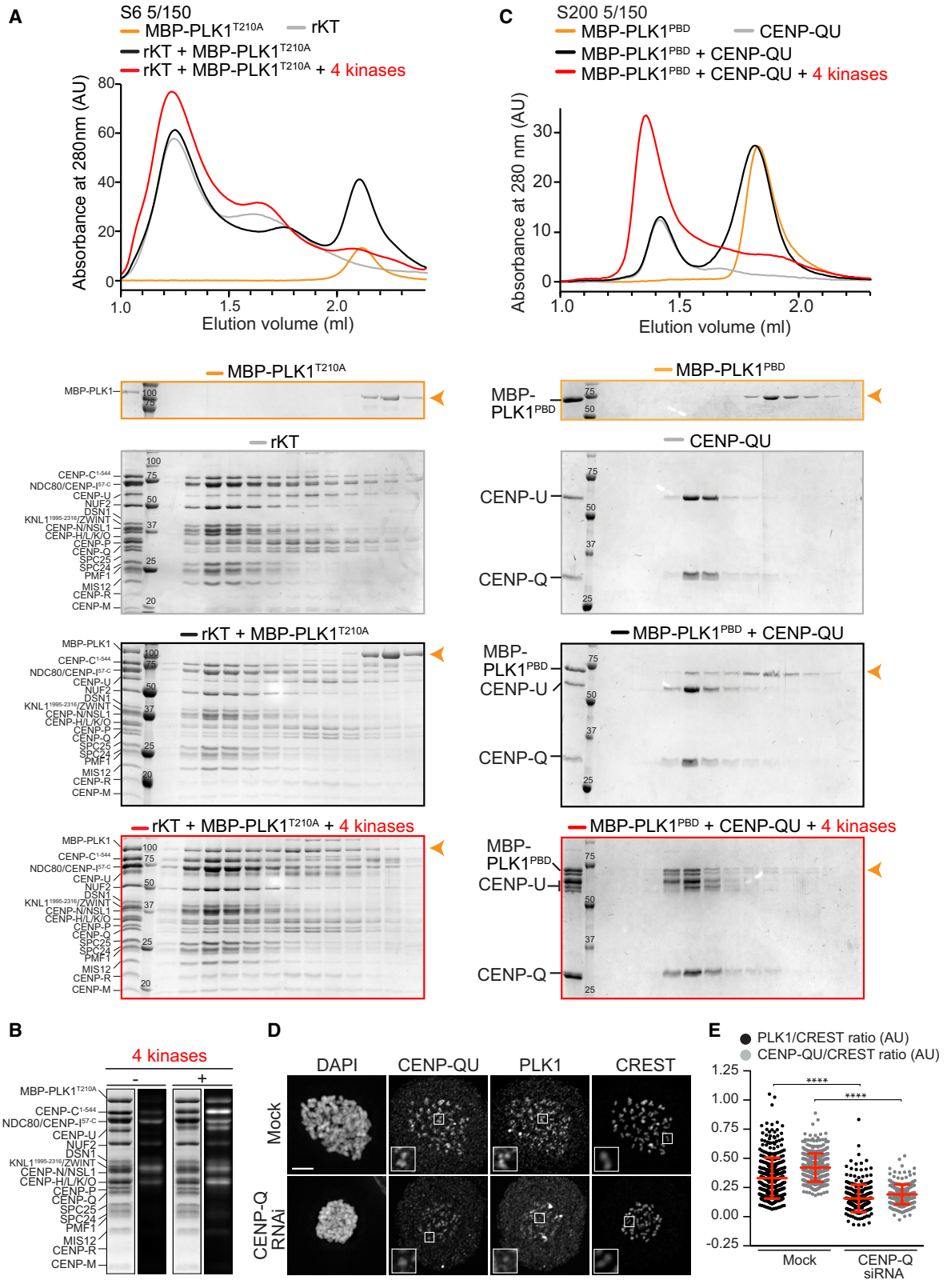


*(legend on next page)*

PLK1 recruitment to this additional receptor(s) was strictly dependent on Aurora B activity because it was strongly inhibited by hesperadin (Figure S2H).

## PLK1 Binds to the Core Kinetochore

To identify the additional PLK1 receptor(s), we reconstituted recombinant kinetochore particles (rKTs) containing 22 subunits, most of inner and outer kinetochore proteins (Figure S5A; note that, for these reconstitutions, we used a C-terminal fragment of KNL1 devoid of BUB1 or BUBR1 binding sites) (Pesenti et al., 2018; Weir et al., 2016). We combined the rKT with MBP-PLK1$^{T210A}$, a recombinant fusion of MBP with an inactive (or very poorly active) mutant of PLK1 (Jang et al., 2002b; Kelm et al., 2002). Aurora B, BUB1, PLK1, and CDK1 were then incubated with rKTs as putative priming kinases, and the resulting mixes were analyzed by SEC. When MBP-PLK1$^{T210A}$ was combined with rKTs without priming kinases, its elution volume did not shift (Figure 3A). Conversely, a complete shift in elution volume was observed with priming kinases, indicating that they generate binding sites for MBP-PLK1$^{T210A}$ on the rKT. Pro-Q Diamond staining revealed background levels of phosphorylation on some rKT subunits, which are generated in insect cells (Figure 3B). Priming kinases caused prominent increases in phosphorylation on only a few rKT subunits, most notably CENP-C (represented by its first 544 residues, CENP-C$^{1–544}$), CENP-U, and the MBP-PLK1$^{T210A}$ fusion itself (Figures 3B and S5B).

With the exception of BUB1:BUB3, the other kinases phosphorylated the rKT individually (Figure S5B). To bypass the confounding factor that PLK1$^{T210A}$ may deliver residual kinase activity at stoichiometric concentrations, we repeated the binding experiments with fluorescent MBP-PLK1$^{PBD}$, testing its interaction with rKT in the presence of individual priming kinases (Figure S3B). Occasionally, the CENP-OPQUR sub-complex detaches from the rKTs in SEC runs and elutes in a separate peak of larger elution volume. Remarkably, priming phosphorylation by PLK1 or CDK1, but not by Aurora B or BUB1:BUB3, promoted co-elution of MBP-PLK1$^{PBD}$ with this CENP-OPQUR peak (Figure S3B). Thus, we asked whether PLK1 also interacts with the CENP-OPQUR complex in the absence of other rKT subunits. At equimolar concentrations (5 μM), the MBP-PLK1$^{PBD}$ and the 5-subunit CENP-OPQUR complex (Pesenti et al., 2018) did not co-elute from a SEC column, whereas a stoichiometric complex was assembled after pre-incubation with priming kinases (Figure S3C). Further SEC analyses demonstrated that the CENP-QU sub-complex was sufficient for a phosphorylation-dependent interaction with MBP-PLK1$^{PBD}$ (Figure 3C), whereas MBP-PLK1$^{PBD}$ did not bind the CENP-OP sub-complex (Figure S3D). Individual CENP-OPQUR subunits are unstable and could not be tested (Pesenti et al., 2018).

Within CENP-OPQUR, CENP-U is a target of priming PLK1, CDK1, or Aurora B (but not BUB1) and is even more pervasively phosphorylated after their combination (Figures 3B, S5B, and S5C). When we pre-incubated the CENP-OPQUR complex with individual priming kinases, only PLK1 (mildly) or CDK1 (strongly) stimulated binding of MBP-PLK1$^{PBD}$ to CENP-OPQUR, whereas Aurora B and BUB1 did not (Figure S5D). Thus, CDK1, and to a lesser extent PLK1, create binding sites for the MBP-PLK1$^{PBD}$ on CENP-QU *in vitro*.

RNAi-based depletion of CENP-Q prevents kinetochore recruitment of the entire CENP-OPQUR without affecting other kinetochore subunits (Pesenti et al., 2018). It also caused a strong reduction of PLK1 kinetochore levels (Figures 3D and 3E). RNAi-based depletion of CENP-Q was not uniform in the cell population, but there was good correlation between residual CENP-Q and PLK1 levels at kinetochores (Figures S6A and S6B). We surmise, however, that in addition to possible variations in individual cells, residual kinetochore PLK1 under these conditions is recruited by BUB1 (and BUBR1), whose levels are unaffected by CENP-OPQUR depletion (Figures S2I–S2L).

## Recruitment of PLK1 to CENP-U at an Ectopic Site

Thr78 of CENP-U$^{PBIP1}$ has been previously identified as a PLK1 target and docking site (Kang et al., 2011; Kang et al., 2006; Kettenbach et al., 2011). Thus, we initially focused on CENP-U to investigate the molecular basis of PLK1 docking. Human CENP-U consists of 418 residues (Figure S6C). Its N-terminal ~115 residues, which have a high-disorder probability and may be unstructured, are not required for kinetochore localization, because a chimeric CENP-U construct encompassing residues 115–418 fused to eGFP was sufficient for kinetochore recruitment. Conversely, a GFP chimera encompassing CENP-U$^{1–114}$ failed to reach kinetochores (Figure 4A).

We asked whether chimeric constructs containing CENP-U or its fragments fused with the LacI repressor were sufficient for targeting PLK1 to an ectopic array of LacO operator sites in an engineered U2OS cell line (Janicki et al., 2004). Full-length (FL) CENP-U or deletion constructs of CENP-U tagged with LacI-EGFP were transiently expressed in these cells for 48 h. Nocodazole (330 nM) was then added for 15–16 h to synchronize cells in mitosis. All LacI-EGFP-CENP-U constructs localized to the ectopic LacO array (Figure 4B). LacI-EGFP-CENP-U$^{1–418}$

**Figure 3. PLK1 Binds CENP-U in the Core Kinetochore**

(A) Elution profile and SDS-PAGE analysis of analytical SEC runs on a Superose 6 increase 5/150 (S6 5/150) column. A mixture of rKT (5 μM) and MBP-PLK1$^{T210A}$ (5 μM) was treated without or without CDK1:cyclin-B, PLK1, Aurora B, and BUB1 (used at 1/20 ratio to target proteins). The orange arrows indicate MBP-PLK1$^{T210A}$.

(B) Phosphorylation of input proteins of the SEC experiment in (A) was assessed by SDS-PAGE, followed by Coomassie or Pro-Q Diamond staining.

(C) Elution profile and SDS-PAGE analysis of analytical SEC runs on a Superdex 200 increase 5/150 (S200 5/150) column of a mixture of CENP-QU subcomplex (5 μM) and MBP-PLK1$^{PBD}$ (5 μM) with or without the same kinases used in (B). Orange arrows highlight MBP-PLK1$^{PBD}$. The MBP-PLK1$^{PDB}$ control is also displayed in Figure S3C.

(D) Representative cells of mock and CENP-Q depleted (using RNAi) HeLa cells immunostained for DAPI, CENP-QU complex, PLK1, and CREST. Scale bar, 5 μm. Small insets frame kinetochores in individual channels.

(E) Dot plots representing PLK1/CREST (black bars) or CENP-QU/CREST (gray bars) kinetochore intensity ratios. Error bars represent means ± standard errors of the mean. A total of 377 kinetochores for mock and 257 kinetochores for CENP-QU-depleted cells in five to six cells were scored.

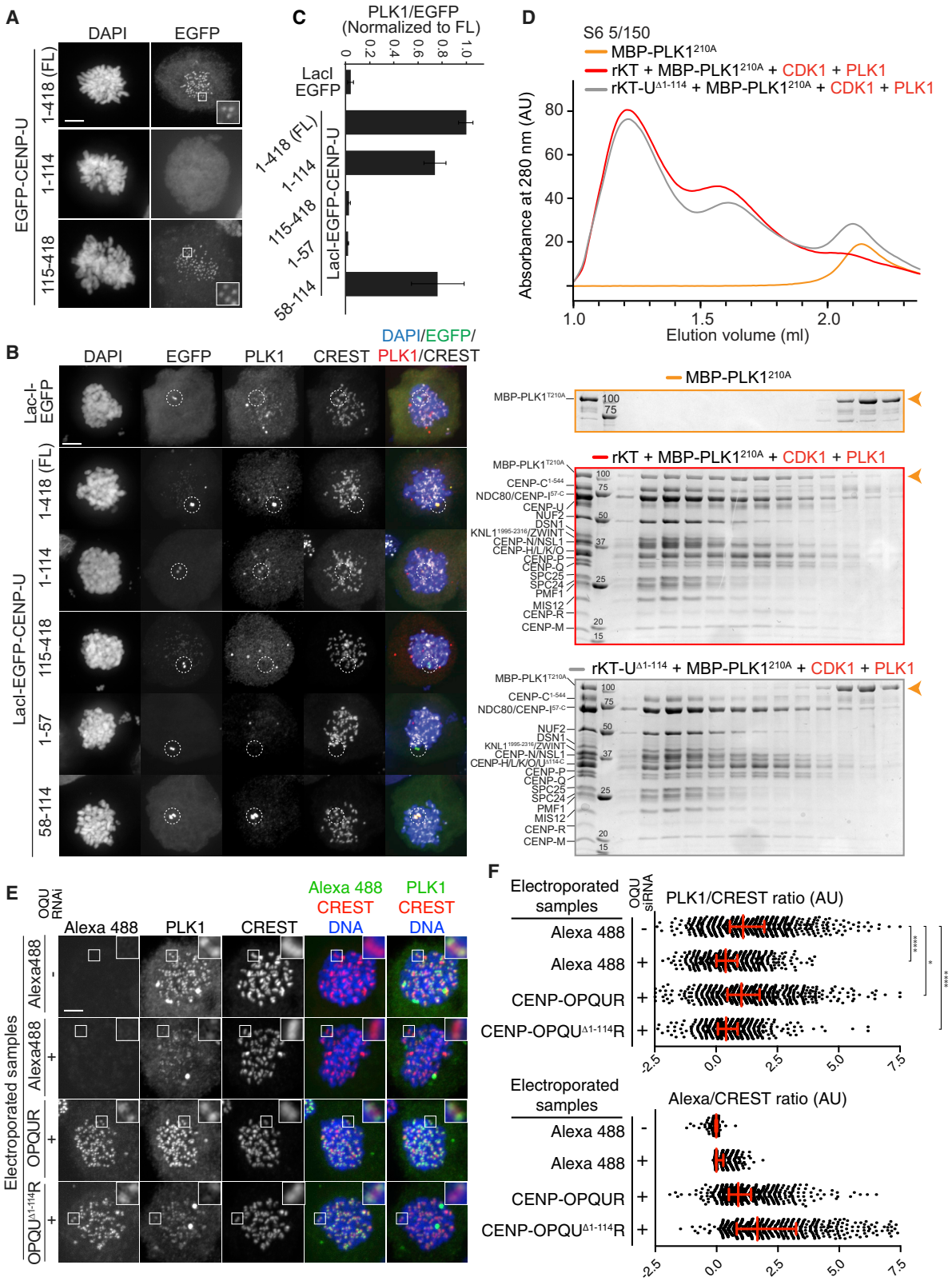


*(legend on next page)*

promoted effective recruitment of PLK1 to the ectopic site, whereas LacI-EGFP-CENP-U$^{115–418}$ did not (Figures 4B, 4C, and S6D). Conversely, LacI-EGFP-CENP-U$^{1–114}$ was sufficient for ectopic localization of PLK1 (Figures 4B and 4C). To map the PLK1 binding site even more precisely, we trimmed CENP-U$^{1–114}$ into two segments, CENP-U$^{1–57}$ and CENP-U$^{58–114}$. CENP-U$^{58–114}$ was sufficient to recruit PLK1 to the ectopic LacO array (Figures 4B, 4C, and S6E). Further trimming resulted in two segments, CENP-U$^{58–85}$ and CENP-U$^{86–114}$, which were unable to recruit PLK1 (Figure S6F). Thus, CENP-U$^{58–114}$ is necessary and sufficient for the interaction of PLK1 to an ectopic chromosome site (Figure S6G).

## CENP-U Is the Sole PLK1 Receptor of Reconstituted Kinetochores

In SEC experiments, recombinant CENP-OPQUR lacking the CENP-U N-terminal region (CENP-OPQU$^{\Delta1–114}$R) did not co-elute with MBP-PLK1$^{PBD}$ in the presence of priming kinases (Figure S7A). As in Figure 3A, MBP-PLK1$^{T210A}$ co-eluted with rKTs phosphorylated by mitotic kinases but failed to co-elute with rKTs reconstituted with CENP-OPQU$^{\Delta1–114}$R (Figure 4D). Thus, the N-terminal region of CENP-U contains the only prominent binding site for PLK1 within rKTs. The phosphorylation pattern of wild-type (WT) and mutant rKTs showed that wild-type CENP-U was effectively phosphorylated, whereas CENP-U$^{\Delta1–114}$ was not (Figure S7B), suggesting that MBP-PLK1$^{T210A}$ interacts directly with the N-terminal fragment of CENP-U after its phosphorylation by CDK1 and PLK1. Thus, we depleted the CENP-OPQUR complex by RNAi (Method Details; Figures S6H–S6J) and replaced it with electroporated recombinant Alexa-488-labeled CENP-OPQUR complexes containing CENP-U$^{WT}$ or CENP-U$^{\Delta1–114}$ (Figures 4E and 4F). As expected, the CENP-U$^{WT}$-containing complex, but not the CENP-U$^{\Delta1–114}$-containing complex, restored high PLK1 kinetochore levels.

## BUB1, BUBR1, and CENP-U as the Only PLK1 Receptors in the Core Kinetochore

Forced kinetochore localization of the CPC restores high kinetochore levels of PLK1 in the absence of BUB1 (Figure 2). A rescue of PLK1 levels in BUB1-depleted cells was also observed upon addition of OA (Figures 5A and 5B), linking PLK1 depletion to dysregulation of phosphatase activity when the BUB1-Aurora B axis is perturbed. Thus, BUB1 has a dual role as a direct PLK1 receptor and as a fulcrum of a confined, but poorly understood, homeostatic phosphorylation network whose abrogation enhances phosphatase activity. Counteracting the latter with OA exposes additional kinetochore receptors of PLK1, at least one of which is CENP-U (Figures 3D, 3E, 5A, and 5B). If CENP-U were the only remaining PLK1 receptor at kinetochores, then, its depletion when the BUB1 axis is disrupted in the presence of OA ought to ablate PLK1 recruitment entirely. In agreement with that, double-depletion of BUB1 and of the CENP-OPQUR complex resulted in complete loss of the kinetochore PLK1. The kinetochore levels of PLK1 under those conditions were comparable to those observed when only BUB1 had been depleted. In contrast with the latter condition, however, no rescue of PLK1 was observed in the double depletion of BUB1 and CENP-OPQUR after addition of OA, indicating that there are no additional major PLK1 receptors (Figures 5A, 5B, and S6K). Conversely, depletion of BUBR1 led to an only marginal co-depletion of kinetochore PLK1, in agreement with previous studies (Cordeiro et al., 2020; Elowe et al., 2007; Ikeda and Tanaka, 2017). We conclude that BUB1 and CENP-U represent the two main kinetochore recruitment axes for PLK1 in nocodazole-arrested cells.

## Role of Thr78 and Thr98 in Kinetochore Recruitment of PLK1

No binding of MBP-CENP-U$^{58-114}$ to PLK1$^{PBD}$ was observed in SEC experiments in the absence of priming kinases (Figure S7C), but pre-phosphorylation of MBP-CENP-U$^{58-114}$ with CDK1 led to complex assembly. Addition of PLK1 promoted a more modest shift in the elution profile of MBP-CENP-U$^{58-114}$ and PLK1$^{PBD}$, suggesting a weak interaction, whereas combination of priming PLK1 and CDK1 caused a robust shift (Figure S7C). Thus, residues 58–114 of CENP-U are sufficient to bind the PBD of PLK1 through CDK1 priming. Although MPS1 and PLK1 share similar target sequences (Dou et al., 2011), MPS1 did not phosphorylate MBP-CENP-U$^{58–114}$ (Figure S4I) and did not promote binding of PLK1$^{PBD}$ to MBP-CENP-U$^{58–114}$ (Figure S4J).

We phosphorylated MBP-CENP-U$^{58–114}$ with PLK1 or CDK1 and analyzed the products by mass spectrometry. CDK1 and

**Figure 4. The CENP-U N Terminus Recruits PLK1**

(A) Representative images of HeLa cells stably expressing doxycycline-inducible constructs of EGFP-CENP-U. Cells were stained with DAPI. EGFP signal is also shown.

(B) Representative images showing U2OS-LacO cells, transiently expressing LacI-EGFP or LacI-EGFP-CENP-U (full-length or deletions). Cells were immunostained for DAPI, PLK1, and CREST. EGFP represent ectopic chromatin location of LacI-EGFP-CENP-U (white circles). Scale bar, 5 μm.

(C) Bar graph shows mean PLK1/CREST intensity at an ectopic location after background subtraction. Each condition was normalized to the signal of the full-length construct. Error bars represent means ± standard errors of the mean. Six to 17 cells were used for quantification, and the experiment was repeated at least three times.

(D) Elution profile and SDS-PAGE analysis of SEC runs of a mixture of rKT and MBP-PLK1$^{T210A}$ (both at 5 μM, red curve) or rKT containing N-terminally deleted CENP-U (rKT-U$^{\Delta1–114}$) and MBP-PLK1$^{T210A}$ (both at 5 μM, gray curve) in the presence of the priming kinases CDK1:cyclin-B and PLK1. Orange arrows highlight MBP-PLK1$^{T210A}$ in each gel.

(E) Representative images of HeLa cells electroporated with CENP-OPQRU$^{WT}$ or CENP-OPQRU$^{\Delta1–114}$ and depleted of endogenous CENP-OPQRU complex by RNAi depletion of CENP-Q, O, U (see Method Details). After siRNA transfection, cells were electroporated with recombinant Alexa-488-labeled CENP-OPQUR complexes, arrested in mitosis with nocodazole and prepared for immunofluorescence. Scale bar, 5 μm.

(F) Dot plots of control normalized PLK1/CREST (top) or Alexa/CREST kinetochore intensity ratio (bottom). Red lines indicate median with interquartile range; 961 kinetochores were scored for mock cells. For CENP-OQU-depleted cells, 782 kinetochores were scored for control Alexa 488 electroporation, 972 for OPQRU$^{WT}$ and 806 for CENP-OPQRU$^{\Delta1–114}$ in 11 to 12 cells per condition.

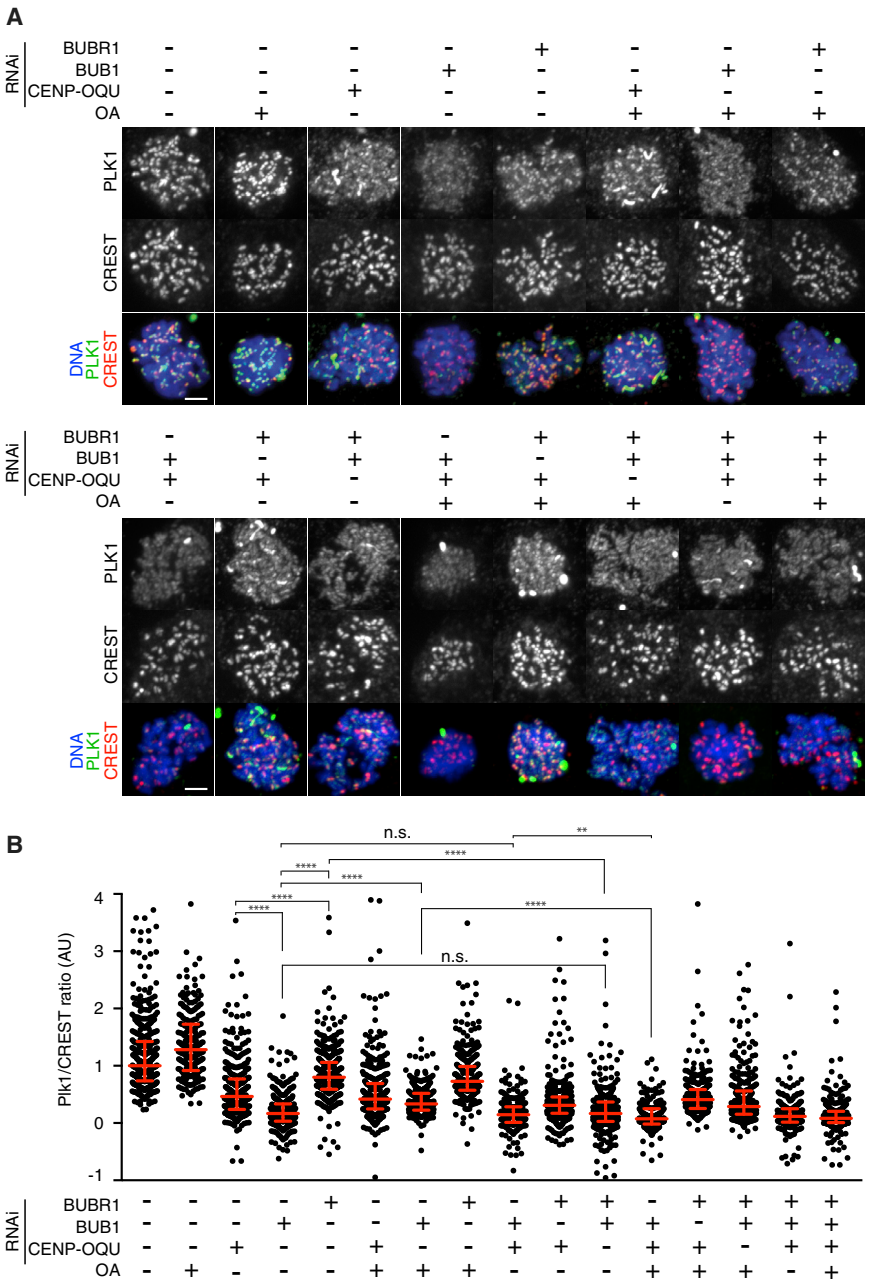


**Figure 5. BUB1/BUBR1 and CENP-U Are the Main PLK1 Kinetochore Recruitment Axes**

(A) Representative images of mitotic HeLa cells depleted for the indicated endogenous proteins and treated with okadaic acid (OA) are indicated. Scale bar, 5 μm.

(B) Dot plots show individual kinetochore quantification of control-normalized PLK1/CREST intensity ratios for cells in (A). Red lines represent median and interquartile range, respectively. Between 233 and 482 kinetochores in 5 to 15 cells were scored for each condition.

PLK1 phosphorylated Thr98 and Thr78, respectively (Figure 6A). Thr98 sits within a classic Ser-Thr-Pro CDK1 consensus site and an ideal recognition motif for the PBD (Elia et al., 2003a) and has been previously identified in a large-scale proteomic analysis (Zhou et al., 2013). Co-incubation with CDK1 and PLK1 did not alter the intensity of the pThr98 signal but led to a significant increase in the stoichiometry of the previously identified PLK1 site Thr78 (Kang et al., 2011; Kang et al., 2006), suggesting that Thr98, after CDK1 phosphorylation, promotes PLK1 binding and, in turn, enhances phosphorylation of Thr78 (Figure 6A). Alanine mutants at Thr78 or Thr98 within MBP-CENP-U$^{58–114}$ demonstrated exquisite specificity of PLK1 and CDK1 for Thr78 and Thr98, respectively (Figure 6B).

To investigate how Thr78 and Thr98 influence PLK1 binding to CENP-U, we phosphorylated MBP-CENP-U$^{58–114}$-S77A/T78A or MBP-CENP-U$^{58–114}$-T98A in subsequent steps with priming CDK1 and PLK1. Pre-treated with CDK1 and PLK1, MBP-CENP-U$^{58–114}$ co-eluted in a stoichiometric complex with MBP-PLK1$^{PBD}$ from a SEC column (Figure 6C). MBP-CENP-U$^{58–114}$-T98A or MBP-CENP-U$^{58–114}$-S77A/T78A, similarly pre-treated, also interacted with MBP-PLK1$^{PBD}$ but eluted with greater elution volume, indicative of a weaker, rapidly dissociating interaction and/or of a different complex stoichiometry. We expressed wild-type EGFP-CENP-U, EGFP-CENP-U-T98A, or EGFP-CENP-U-S77A/T78A in HeLa cells and measured the kinetochore levels of PLK1 (Figures 6D, 6E, and S6L). Both mutants caused a significant reduction in kinetochore PLK1 levels in comparison to wild-type CENP-U, providing evidence for a cellular role of Thr78 and Thr98 in PLK1 recruitment. Thus, CDK1 primes binding of PLK1 to CENP-U through phosphorylation of Thr98, which PLK1 may then use as an initial binding platform to create a stable docking configuration. As a side note, PLK1 recruitment to the ectopic LacO site was independent of cell-cycle stage (Figures S6D–S6F). This may seem inconsistent with a crucial role of CDK1, but we note that this assay may not faithfully recapitulate the conditions of kinetochores in which counteracting phosphatases are enriched.

## PLK1 Dimerization on CENP-U

Finally, we investigated whether the requirement for PLK1 and CDK1 for robust recruitment of PLK1 to T78 and T98 reflected binding of distinct PLK1 molecules to the two sites. To assess that, we incubated, in 3-fold excess to saturate binding sites,

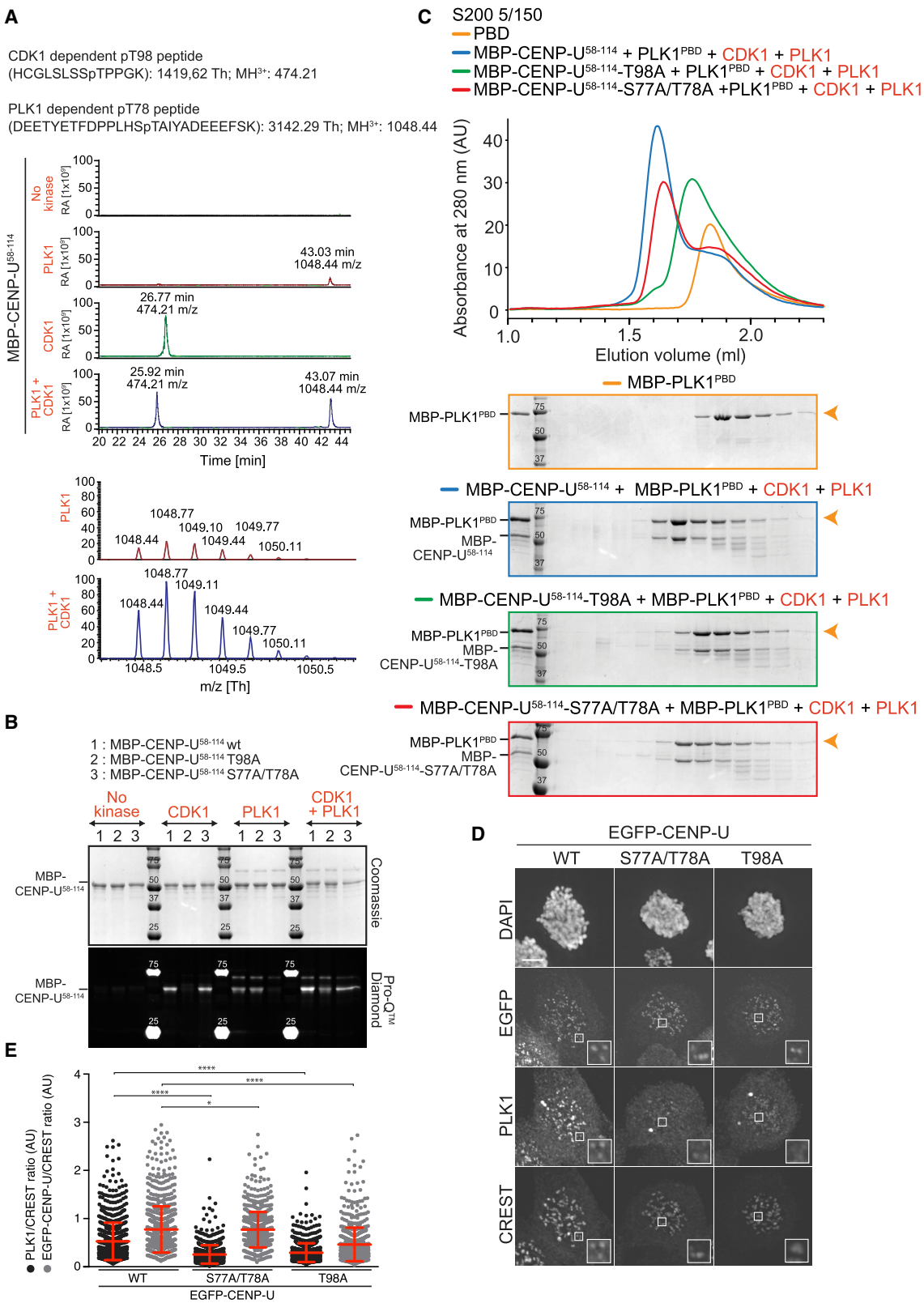


*(legend on next page)*

fluorescently labeled MBP-PLK1$^{T210A}$ and CENP-OPQUR in the presence of CDK1 and PLK1 as priming kinases. We then isolated the resulting complex by SEC and estimated its mass by sedimentation velocity analytical ultracentrifugation (AUC; Figures 7A and S7D). The MBP-PLK1$^{210A}$:CENP-OPQUR complex had a sedimentation coefficient of 7.6 S and an apparent molecular mass of 387.6 kDa, in excellent agreement with the predicted molecular mass for a complex of two MBP-PLK1$^{210A}$ molecules and one CENP-OPQUR (385.1 kDa). These results indicate that two molecules of PLK1 bind phosphorylated CENP-U.

## DISCUSSION

Here, we answer a long-standing question on the molecular mechanism of PLK1 recruitment to kinetochores. Through a combination of *in vitro* reconstitution and cellular work, we corroborate previous evidence that PLK1 interacts with BUB1 and BUBR1 and demonstrate that the N-terminal region of CENP-U is the sole robust binding site for PLK1 within the core kinetochore (Figure 7B). The reconstituted kinetochores used in our studies incorporate most kinetochore subunits, generally in full-length form. Some segments, however, have been removed because of poor expression or instability of the full-length proteins. The largest single missing segment is the N-terminal region of KNL1, a protein that is only represented in our reconstitutions by the C-terminal 1995 to 2316 residues. Residues 1–56 of CENP-I and 545–943 of CENP-C are also missing (Pesenti et al., 2018; Weir et al., 2016). Because depletion of the CENP-OPQUR complex in human cells does not affect the localization of CENP-C and CENP-I (Pesenti et al., 2018), whereas it leads to complete disappearance of PLK1 from kinetochores when BUB1 is co-depleted (this study), we conclude that most PLK1 in the core kinetochore is recruited to CENP-U. The proposed localization of PLK1 at a defined location internal (i.e., more chromatin proximal) to CENP-I (Lera et al., 2016) is indeed consistent with the expected position of the CENP-QU subcomplex revealed by recent structural work (Hinshaw and Harrison, 2019; Pesenti et al., 2018; Yan et al., 2019). We cannot exclude the possibility that PLK1 recruitment to BUB1 and CENP-U activates downstream phosphorylation events that promote hierarchical recruitment of PLK1 to additional receptors, thus explaining the plethora of different potential PLK1 kinetochore receptors previously identified (see Introduction). Because our PLK1 localization experiments were performed in nocodazole, i.e., in the absence of microtubules, they do not exclude recruitment of PLK1 to additional receptors generated after recruitment of "late" kinetochore residents, such as the SKA and SKAP complexes (Wimbish and DeLuca, 2020).

We show that CDK activity is required for PLK1 recruitment to mitotic kinetochores, extending a previous proposal that PLK1's binding to CENP-U is exclusively primed by PLK1 itself (Kang et al., 2006, 2011). The self-priming model proposed that PLK1 phosphorylates Thr78 of CENP-U and subsequently docks onto that site (Kang et al., 2011; Kang et al., 2006). Importantly, our observations are not inconsistent with self-priming because we confirm that PLK1 phosphorylates, and docks onto, Thr78. However, we show that kinetochore recruitment of PLK1 is, in addition, also CDK1 dependent. Combining PLK1 and CDK1 inhibitors essentially eliminated kinetochore PLK1 (Figures 2E and 2F).

As already observed, self-priming may be the prevalent mechanism of PLK1 interaction with its targets in anaphase, such as PRC1, a key regulator of cytokinesis that cross-links anti-parallel microtubules. Dissection of the mechanism of PLK1 binding to PRC1 in anaphase has focused on two closely spaced Ser-Thr-X (with X ≠ proline) PLK1 target motifs on PRC1 (Neef et al., 2007) (Figure 7C). Lacking negative charges at position −2 relative to the phosphorylated Thr, these sites are non-ideal PLK1 substrates (Alexander et al., 2011; Hegemann et al., 2011; Kettenbach et al., 2011; Nakajima et al., 2003). However, they are predicted to be good PBD docking sites in view of the hydrophobic residue (Φ) at position −3 (in magenta in Figures 7C and 7D), which has been shown to increase binding affinity for the PBD (Zhu et al., 2016). After recruitment of the first PLK1 molecule (arbitrarily depicted at the PLK1$_2$ site in Figure 7D, top), stable binding may be achieved after local phosphorylation of the neighboring PLK1$_1$ site, recruitment there of the second PLK1 molecule, and dimerization. There is evidence that the hydrophobic residue at −3 facilitates PBD domain dimerization, further leading to activation of PLK1 kinase activity (Zhu et al., 2016). Similarly spaced, tandem Ser-Thr-X strings are also present in MKLP2, another self-primed anaphase binding partner of PLK1 (Neef et al., 2003), but it is unclear whether this constellation is required for PLK1 localization. Nothing prevents this mechanism from working during mitosis as well. Indeed, pre-anaphase binding of PLK1 to PRC1 is only hindered by CDK1 itself through inhibitory phosphorylation (Neef et al., 2007).

The interdependence of CDK1 and PLK1 kinase activity for PLK1 kinetochore recruitment to its mitotic receptors needs to

**Figure 6. CDK1 and PLK1 Prime PLK1 Interaction with the CENP-U N-Terminal Region**

(A) Profiles of consecutive MS runs of the pT98 and pT78 containing CENP-U peptides. The relative abundance (RA, y axis) was set for all runs to 1 × 10E$^9$ (top). Isotopic pattern of the MS1 spectra of the pT78 containing peptide incubated only with PLK1 (upper spectrum) and incubated with PLK1 and CDK1 (lower spectrum). MS1 spectra were taken from eluted peaks. The highest peak from both spectra was set to 100%. Data were directly extracted from Xcalibur (bottom).

(B) Phosphorylation state of CENP-U$^{58-114}$ wild-type, S77A/T78A, or T98A upon phosphorylation by CDK1:cyclin B and/or PLK1 kinases was assessed using SDS-PAGE followed by Pro-Q Diamond and Coomassie staining.

(C) Elution profile and SDS-PAGE of analytical SEC runs of MBP-PLK1$^{PBD}$ alone (orange) and of mixtures of CENP-U$^{58-114}$ wild-type, S77A/T78A, or T98A (5 μM) with MBP-PLK1$^{PBD}$ (5 μM) in the presence of PLK1 and/or CDK1:cyclinB (blue, green, and red curves, respectively). The SDS-PAGE and elution profile for the CDK1+PLK1 condition are also displayed in Figure S7C.

(D) Representative images of HeLa cells stably expressing doxycycline-inducible wild-type, S77/T78A, or T98A EGFP-CENP-U, immunostained for DAPI, PLK1, and CREST. Scale bar, 5 μm.

(E) Dot plot of PLK1/CREST (black dots) or EGFP-CENP-U (WT or mutant, gray dots) kinetochore intensity ratios. Error bars represent means ± standard errors of the mean; 910 kinetochores for WT, 791 for S77/T78A, and 797 for T98A mutant, belonging to 14–17 different cells, were scored.

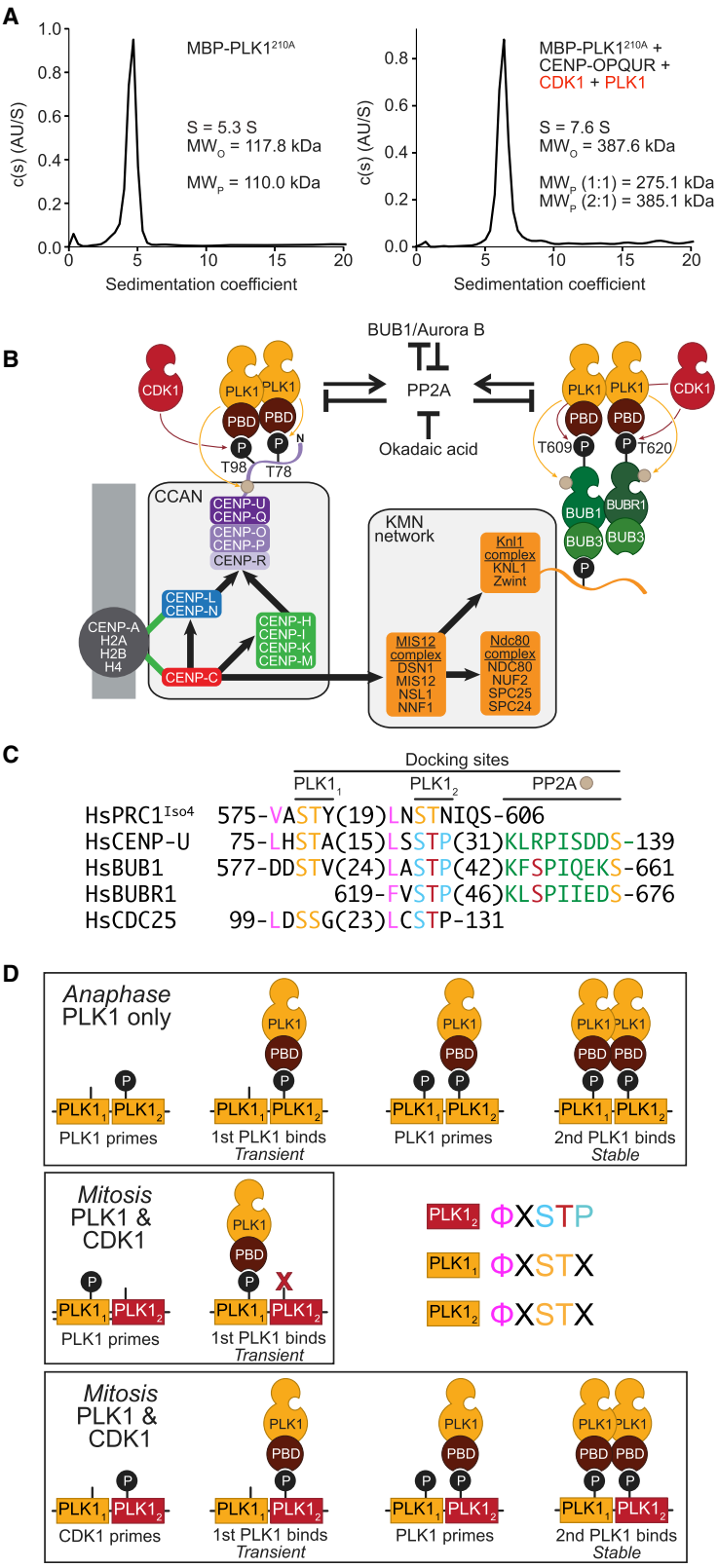


**Figure 7. Docking and Dimerization of PLK1 on Target Proteins**

(A) Sedimentation velocity AUC monitoring absorbance of fluorescent MBP-PLK1$^{T210A}$. MBP-PLK1$^{T210A}$ bound to CENP-OPQUR complex in 2:1 ratio in the presence of catalytic amounts of PLK1, CDK1, and ATP-$Mg^{2+}$.

(B) Scheme of main findings on the mechanism of kinetochore recruitment of PLK1.

(C) Sequence alignment of various mitotic and post-anaphase receptors of PLK1. PLK1 substrate sites or motifs are in yellow; CDK target sites in red within a blue motif; a hydrophobic residue enhancing target binding and dimerization is in magenta; PP2A-B56 docking motif is in green. Numbers in parentheses indicate residues in sequence gaps.

(D) Models for kinetochore recruitment of PLK1 at anaphase and mitosis.

explain (1) the requirement for CDK1, and (2) why PLK1 is insufficient to self-prime its own recruitment to these proteins. The PLK1 recruitment sites on BUB1 and CENP-U resemble the PRC1 constellation (Figure 7B), suggesting that the CDK1-PLK1 interdependence may be achieved through a variation on the theme of the PRC1 recruitment model. The most notable difference is that, in BUB1 and CENP-U, there are Ser-Thr-Pro sites at the $PLK1_2$ position, whereas a Ser-Thr-X sequence remains at the $PLK1_1$ site (not in BUBR1, however). Because proline versus non-proline specificity in the P+1 position of protein kinases are mutually exclusive properties (Canagarajah et al., 1997; Songgyang et al., 1996), initial docking of PLK1 to the Ser-Thr-X $PLK1_1$ site will fail to lead to phosphorylation of the Ser-Thr-Pro $PLK1_2$ site. This will prevent recruitment of a second molecule of PLK1 and stabilization of binding, thus explaining why self-priming does not work with this constellation (Figure 7D, middle). Conversely, initial phosphorylation by CDK1 of the Ser-Thr-Pro site at $PLK1_2$ will ignite recruitment of PLK1, followed by successful phosphorylation of the Ser-Thr-X site at $PLK1_1$, recruitment of a second PLK1 molecule, and stabilization by dimerization, explaining the requirement for CDK1 (Figure 7D, bottom). Indeed, CDK1 phosphorylation at Thr98 facilitates the phosphorylation of the non-ideal substrate Thr78 (Figure 6A). Furthermore, dimerization of PLK1 (presumably through the PBDs) explains why both CDK1 and PLK1 are necessary for a full shift of the PBDs with CENP-U (Figure 6C). This recruitment model for PLK1 involves motifs predicted not to be ideal targets of the catalytic domain, thus predicting that strong physical interactions with PLK1 are limited to proteins that provide a defined constellation of PBD binding sites, but also that the range of PLK1 kinase substrates may be significantly larger.

Sequential CDK1-PLK1 phosphorylation has been observed with various PLK1 substrates, including NEK9, NEDD1, Caspase8, and CDC25 (Bertran et al., 2011; Lobjois et al., 2011; Matthess et al., 2014; O'Donovan et al., 2013; Zhang et al., 2009). The model we are proposing does not require a specific order for the $PLK1_1$ and $PLK1_2$ motifs, but only that they are spatially adjacent to permit dimerization. We note, however, that several other known or potential PLK1-binding partners, including Meikin and BuGZ (Jiang et al., 2014; Kim et al., 2015), have constellations of CDK1 and PLK1 that closely resemble those of BUB1 and CENP-U (unpublished data).

Aurora B is crucial for kinetochore-microtubule attachment and mitotic checkpoint signaling, and it is important to address whether INCENP and other subunits of the CPC contribute to PLK1 recruitment as proposed (Goto et al., 2006; Sun et al., 2012). The CPC is predominantly centromeric and, therefore, extends into a domain that is precluded to PLK1, whose microscopic distribution is limited to kinetochores (this study and many others, including, for instance, Lénárt et al. [2007] and Lera et al. [2016]). It is possible, however, that the interaction is limited to kinetochore-confined pools of these proteins. Arguing against that idea, in the presence of priming kinases and under conditions similar to those that promote robust interactions of PLK1 with BUB1 or CENP-U, we failed to observe direct binding of the CPC and PLK1 (M.P. and A.M., unpublished data). Thus, the CPC may contribute to the recruitment of BUB1 through the kinase activity of Aurora B, as previously proposed (Qi et al., 2006) and confirmed here (Figure S2H). The requirement for Aurora B was bypassed by inhibition of protein phosphatases (Figure 2A), suggesting that Aurora B regulates the balance of kinase and phosphatase activity required for optimal PLK1 recruitment.

Dynamic regulation of kinase-phosphatase switches within kinetochores, including those involving PLK1, is crucial for kinetochore-microtubule attachment and spindle assembly checkpoint but remains very poorly understood (Cordeiro et al., 2020; Elowe et al., 2007, 2010; Ikeda and Tanaka, 2017; Jia et al., 2016; Kaisari et al., 2019; Lénárt et al., 2007; Liu et al., 2012; Maia et al., 2012; Moutinho-Santos et al., 2012; O'Connor et al., 2015; Peters et al., 2006; von Schubert et al., 2015). High PLK1 activity at kinetochores in prometaphase stabilizes kinetochore microtubules and balances a destabilizing activity attributed to Aurora B (Foley et al., 2011; Liu et al., 2012). PLK1 has been previously implicated in the control of PP2A activity (Joukov and De Nicolo, 2018; Saurin, 2018) through the creation of docking sites for the B56 regulatory subunit on BUB1 and BUBR1 (Cordeiro et al., 2020; Elowe et al., 2007; Hertz et al., 2016; Kruse et al., 2013; Suijkerbuijk et al., 2012b). MYPT1, a PP1 regulator and a CDK1:cyclin A substrate, has instead emerged as a potential negative regulator of PLK1 (Dumitru et al., 2017; Yamashiro et al., 2008).

When we were scanning the sequence of human CENP-U, we realized that it encompasses the same constellation of PLK1 and PP2A-B56 docking sites observed in BUB1 and BUBR1 (Figure 7B). This new observation strongly suggests that CENP-U, like BUB1 and BUBR1, provides a PLK1-regulated docking site for the B56 regulatory subunit, a hypothesis that we are currently testing. We note that, in a previous study, the PP2A regulator BOD1 was implicated in kinetochore recruitment of PLK1 (Porter et al., 2013). We speculate that the CENP-U-associated pool of PP2A-B56 may be directed to two crucial functions of the CENP-OPQUR complex. First, CENP-Q has been implicated in microtubule depolymerization-coupled pulling on kinetochores, (Bancroft et al., 2015). In a previous study, we identified a microtubule binding site in the N-terminal region of CENP-Q, a direct binding partner of CENP-U (Pesenti et al., 2018). As evinced from the structure of their orthologs in *S. cerevisiae*, CENP-Q and CENP-U are predicted to form a parallel coiled-coil structure (Hinshaw and Harrison, 2019; Yan et al., 2019), predicting close proximity of their N-termini and supporting speculations of crosstalk between the microtubule-binding site of CENP-Q and PLK1 activity from the CENP-U docking site. Thus, it will be crucial to assess whether microtubule binding by CENP-Q affects PLK1 recruitment or activity, and if so, how. Second, the CENP-OPQUR complex promotes cohesin recruitment and loading at the centromere in *S. cerevisiae*, and CENP-U has been shown to contain a sequence motif, preceding the PLK1 binding sites, for interaction with the SA2 subunit of cohesin (Fernius and Marston, 2009; Hinshaw et al., 2017; Li et al., 2020; Natsume et al., 2013). PP2A bound to CENP-U may contribute to protect cohesin at centromeres from the so-called prophase pathway that removes cohesin from chromosome arms concomitantly with the individualization of sister chromatids (Haarhuis et al., 2014).

In conclusion, we present a comprehensive analysis of the mechanism of PLK1 recruitment to kinetochores (Figure 7B). We are still far from understanding how the complex interaction of Aurora B and PLK1 kinases and of the PP1, PP2A, and possibly other phosphatases leads to bi-orientation, the stabilization of kinetochore-microtubule attachment, satisfaction of the mitotic checkpoint, and centromere organization. Our attempts to reconstitute *in vitro* these dependencies lay the foundations for surgical molecular manipulations required to dissect their mechanistic basis.

## STAR★METHODS

Detailed methods are provided in the online version of this paper and include the following:

- KEY RESOURCES TABLE
- RESOURCE AVAILABILITY
  - Lead Contact
  - Materials Availability
  - Data and Code Availability
- EXPERIMENTAL MODEL AND SUBJECT DETAILS
  - Cells lines and Expression strains
- METHOD DETAILS
  - Cell transfection and electroporation
  - Plasmids
  - Cell synchronization
  - Immunofluorescence
  - Western blotting
  - Cell imaging
  - Protein expression and purification
  - *In vitro* assembly of rKT and rKT containing CENP-U$^{\Delta 1\text{-}114}$
  - Recombinant proteins fluorescence labeling
  - *In vitro* phosphorylation of rKT, rKT containing CENP-U$^{\Delta 1\text{-}114}$, CENP-OPQUR, -OPQU$^{\Delta 1\text{-}114}$R, -OP, -QU, 6His-MBP-CENP-U$^{58\text{-}114}$-WT and mutants, BUB1:-BUB3 and BUBR1:BUB3
  - Phosphostaining of recombinant proteins
  - Analytical SEC
  - Analytical ultracentrifugation (AUC)
  - Mass spectrometry and phosphorylation site analysis
- QUANTIFICATION AND STATISTICAL ANALYSIS
  - Cell image analysis
  - AUC analysis
  - Mass Spectrometry analysis

## SUPPLEMENTAL INFORMATION

Supplemental Information can be found online at https://doi.org/10.1016/j.molcel.2020.10.040.

## ACKNOWLEDGMENTS

We are grateful to Geert Kops and Andrew McAinsh for sharing tools and reagents; Charlotte M. Smith for sharing oligos for CENP-QU RNAi; Hendrik Hausmann, Ingrid Hoffmann, Carolin Koerner, Lisa Schulze, Isabelle Stender, Doro Vogt, Beate Voss, and Sabine Wohlgemuth for general technical assistance; Valentina Piano and Suruchi Sethi for sharing BUB1:BUB3 and BUBR1:BUB3; Raphael Gasper-Schonenbrucher for help with biophysical experiments; and Adrian Saurin for helpful discussions. A.M. gratefully acknowledges funding by the Max Planck Society, the European Research Council (ERC) Advanced Investigator Grant RECEPIANCE (proposal 669686), and the DFG's Collaborative Research Centre (CRC) 1093. P.S. gratefully acknowledges the support of the Alexander von Humboldt Foundation through a postdoctoral fellowship and is thankful to IIT Jodhpur for the present infrastructure support. P.S. also acknowledges the Science and Engineering Research Board (ECR/2017/001001410) and the Har Gobind Khorana-Innovative Young Biotechnologist Award (BT/12/IYBA/2019/02) for current support.

## AUTHOR CONTRIBUTIONS

P.S., M.E.P., and A.M. conceptualized the study. P.S. and M.E.P. conducted most of the experiments and analyzed data for the work. S.C. and A.P. (biochemistry); A.S., S.M., and M.H. (cell biology); and T.B. (mass spectrometry) assisted P.S. and M.E.P. in experiments and data analysis. P.S. and M.E.P., with help from the other authors, compiled the data for the manuscript. A.M. wrote the manuscript with contributions from all authors.

## DECLARATION OF INTERESTS

The authors declare no competing interests

Received: April 10, 2020
Revised: September 8, 2020
Accepted: October 28, 2020
Published: November 27, 2020

## REFERENCES

Adams, R.R., Wheatley, S.P., Gouldsworthy, A.M., Kandels-Lewis, S.E., Carmena, M., Smythe, C., Gerloff, D.L., and Earnshaw, W.C. (2000). INCENP binds the Aurora-related kinase AIRK2 and is required to target it to chromosomes, the central spindle and cleavage furrow. Curr. Biol. *10*, 1075–1078.

Ahonen, L.J., Kallio, M.J., Daum, J.R., Bolton, M., Manke, I.A., Yaffe, M.B., Stukenberg, P.T., and Gorbsky, G.J. (2005). Polo-like kinase 1 creates the tension-sensing 3F3/2 phosphoepitope and modulates the association of spindle-checkpoint proteins at kinetochores. Curr. Biol. *15*, 1078–1089.

Alex, A., Piano, V., Polley, S., Stuiver, M., Voss, S., Ciossani, G., Overlack, K., Voss, B., Wohlgemuth, S., Petrovic, A., et al. (2019). Electroporated recombinant proteins as tools for in vivo functional complementation, imaging and chemical biology. eLife *8*, e48287.

Alexander, J., Lim, D., Joughin, B.A., Hegemann, B., Hutchins, J.R., Ehrenberger, T., Ivins, F., Sessa, F., Hudecz, O., Nigg, E.A., et al. (2011). Spatial exclusivity combined with positive and negative selection of phosphorylation motifs is the basis for context-dependent mitotic signaling. Sci. Signal. *4*, ra42.

Amaro, A.C., Samora, C.P., Holtackers, R., Wang, E., Kingston, I.J., Alonso, M., Lampson, M., McAinsh, A.D., and Meraldi, P. (2010). Molecular control of kinetochore-microtubule dynamics and chromosome oscillations. Nat. Cell Biol. *12*, 319–329.

Amin, M.A., Itoh, G., Iemura, K., Ikeda, M., and Tanaka, K. (2014). CLIP-170 recruits PLK1 to kinetochores during early mitosis for chromosome alignment. J. Cell Sci. *127*, 2818–2824.

Archambault, V., and Glover, D.M. (2009). Polo-like kinases: conservation and divergence in their functions and regulation. Nat. Rev. Mol. Cell Biol. *10*, 265–275.

Arnaud, L., Pines, J., and Nigg, E.A. (1998). GFP tagging reveals human Polo-like kinase 1 at the kinetochore/centromere region of mitotic chromosomes. Chromosoma *107*, 424–429.

Bancroft, J., Auckland, P., Samora, C.P., and McAinsh, A.D. (2015). Chromosome congression is promoted by CENP-Q- and CENP-E-dependent pathways. J. Cell Sci. *128*, 171–184.

Baron, A.P., von Schubert, C., Cubizolles, F., Siemeister, G., Hitchcock, M., Mengel, A., Schröder, J., Fernández-Montalván, A., von Nussbaum, F.,

Mumberg, D., and Nigg, E.A. (2016). Probing the catalytic functions of Bub1 kinase using the small molecule inhibitors BAY-320 and BAY-524. eLife *5*, e12187.

Bertran, M.T., Sdelci, S., Regué, L., Avruch, J., Caelles, C., and Roig, J. (2011). Nek9 is a Plk1-activated kinase that controls early centrosome separation through Nek6/7 and Eg5. EMBO J. *30*, 2634–2647.

Bialojan, C., and Takai, A. (1988). Inhibitory effect of a marine-sponge toxin, okadaic acid, on protein phosphatases. Specificity and kinetics. Biochem. J. *256*, 283–290.

Bird, A.W., and Hyman, A.A. (2008). Building a spindle of the correct length in human cells requires the interaction between TPX2 and Aurora A. J. Cell Biol. *182*, 289–300.

Breit, C., Bange, T., Petrovic, A., Weir, J.R., Müller, F., Vogt, D., and Musacchio, A. (2015). Role of Intrinsic and Extrinsic Factors in the Regulation of the Mitotic Checkpoint Kinase Bub1. PLoS ONE *10*, e0144673.

Burkard, M.E., Maciejowski, J., Rodriguez-Bravo, V., Repka, M., Lowery, D.M., Clauser, K.R., Zhang, C., Shokat, K.M., Carr, S.A., Yaffe, M.B., and Jallepalli, P.V. (2009). Plk1 self-organization and priming phosphorylation of HsCYK-4 at the spindle midzone regulate the onset of division in human cells. PLoS Biol. *7*, e1000111.

Caldas, G.V., DeLuca, K.F., and DeLuca, J.G. (2013). KNL1 facilitates phosphorylation of outer kinetochore proteins by promoting Aurora B kinase activity. J. Cell Biol. *203*, 957–969.

Canagarajah, B.J., Khokhlatchev, A., Cobb, M.H., and Goldsmith, E.J. (1997). Activation mechanism of the MAP kinase ERK2 by dual phosphorylation. Cell *90*, 859–869.

Carmena, M., Pinson, X., Platani, M., Salloum, Z., Xu, Z., Clark, A., Macisaac, F., Ogawa, H., Eggert, U., Glover, D.M., et al. (2012). The chromosomal passenger complex activates Polo kinase at centromeres. PLoS Biol. *10*, e1001250.

Cheeseman, I.M., Chappie, J.S., Wilson-Kubalek, E.M., and Desai, A. (2006). The conserved KMN network constitutes the core microtubule-binding site of the kinetochore. Cell *127*, 983–997.

Cheng, K.-Y., Lowe, E.D., Sinclair, J., Nigg, E.A., and Johnson, L.N. (2003). The crystal structure of the human polo-like kinase-1 polo box domain and its phospho-peptide complex. EMBO J. *22*, 5757–5768.

Clay, F.J., McEwen, S.J., Bertoncello, I., Wilks, A.F., and Dunn, A.R. (1993). Identification and cloning of a protein kinase-encoding mouse gene, Plk, related to the polo gene of Drosophila. Proc. Natl. Acad. Sci. USA *90*, 4882–4886.

Combes, G., Alharbi, I., Braga, L.G., and Elowe, S. (2017). Playing polo during mitosis: PLK1 takes the lead. Oncogene *36*, 4819–4827.

Cordeiro, M.H., Smith, R.J., and Saurin, A.T. (2020). Kinetochore phosphatases suppress autonomous kinase activity to control the spindle assembly checkpoint. J. Cell Biol. *219*, e202002020.

Cox, J., and Mann, M. (2008). MaxQuant enables high peptide identification rates, individualized p.p.b.-range mass accuracies and proteome-wide protein quantification. Nat. Biotechnol. *26*, 1367–1372.

De Antoni, A., Maffini, S., Knapp, S., Musacchio, A., and Santaguida, S. (2012). A small-molecule inhibitor of Haspin alters the kinetochore functions of Aurora B. J. Cell Biol. *199*, 269–284.

De Luca, M., Lavia, P., and Guarguaglini, G. (2006). A functional interplay between Aurora-A, Plk1 and TPX2 at spindle poles: Plk1 controls centrosomal localization of Aurora-A and TPX2 spindle association. Cell Cycle *5*, 296–303.

DeLuca, J.G., Gall, W.E., Ciferri, C., Cimini, D., Musacchio, A., and Salmon, E.D. (2006). Kinetochore microtubule dynamics and attachment stability are regulated by Hec1. Cell *127*, 969–982.

Dou, Z., von Schubert, C., Körner, R., Santamaria, A., Elowe, S., and Nigg, E.A. (2011). Quantitative mass spectrometry analysis reveals similar substrate consensus motif for human Mps1 kinase and Plk1. PLoS ONE *6*, e18793.

Dumitru, A.M.G., Rusin, S.F., Clark, A.E.M., Kettenbach, A.N., and Compton, D.A. (2017). Cyclin A/Cdk1 modulates Plk1 activity in prometaphase to regulate kinetochore-microtubule attachment stability. eLife *6*, e29303.

Elia, A.E., Cantley, L.C., and Yaffe, M.B. (2003a). Proteomic screen finds pSer/pThr-binding domain localizing Plk1 to mitotic substrates. Science *299*, 1228–1231.

Elia, A.E., Rellos, P., Haire, L.F., Chao, J.W., Ivins, F.J., Hoepker, K., Mohammad, D., Cantley, L.C., Smerdon, S.J., and Yaffe, M.B. (2003b). The molecular basis for phosphodependent substrate targeting and regulation of Plks by the Polo-box domain. Cell *115*, 83–95.

Elowe, S., Hümmer, S., Uldschmid, A., Li, X., and Nigg, E.A. (2007). Tension-sensitive Plk1 phosphorylation on BubR1 regulates the stability of kinetochore microtubule interactions. Genes Dev. *21*, 2205–2219.

Elowe, S., Dulla, K., Uldschmid, A., Li, X., Dou, Z., and Nigg, E.A. (2010). Uncoupling of the spindle-checkpoint and chromosome-congression functions of BubR1. J. Cell Sci. *123*, 84–94.

Fernius, J., and Marston, A.L. (2009). Establishment of cohesion at the pericentromere by the Ctf19 kinetochore subcomplex and the replication fork-associated factor, Csm3. PLoS Genet. *5*, e1000629.

Foley, E.A., Maldonado, M., and Kapoor, T.M. (2011). Formation of stable attachments between kinetochores and microtubules depends on the B56-PP2A phosphatase. Nat. Cell Biol. *13*, 1265–1271.

García-Alvarez, B., de Cárcer, G., Ibañez, S., Bragado-Nilsson, E., and Montoya, G. (2007). Molecular and structural basis of polo-like kinase 1 substrate recognition: Implications in centrosomal localization. Proc. Natl. Acad. Sci. USA *104*, 3107–3112.

Golsteyn, R.M., Schultz, S.J., Bartek, J., Ziemiecki, A., Ried, T., and Nigg, E.A. (1994). Cell cycle analysis and chromosomal localization of human Plk1, a putative homologue of the mitotic kinases Drosophila polo and Saccharomyces cerevisiae Cdc5. J. Cell Sci. *107*, 1509–1517.

Girdler, F., Sessa, F., Patercoli, S., Villa, F., Musacchio, A., and Taylor, S. (2008). Molecular basis of drug resistance in aurora kinases. Chem. Biol. *15*, 552–562.

Golsteyn, R.M., Mundt, K.E., Fry, A.M., and Nigg, E.A. (1995). Cell cycle regulation of the activity and subcellular localization of Plk1, a human protein kinase implicated in mitotic spindle function. J. Cell Biol. *129*, 1617–1628.

Goto, H., Kiyono, T., Tomono, Y., Kawajiri, A., Urano, T., Furukawa, K., Nigg, E.A., and Inagaki, M. (2006). Complex formation of Plk1 and INCENP required for metaphase-anaphase transition. Nat. Cell Biol. *8*, 180–187.

Haarhuis, J.H., Elbatsh, A.M., and Rowland, B.D. (2014). Cohesin and its regulation: on the logic of X-shaped chromosomes. Dev. Cell *31*, 7–18.

Hanisch, A., Wehner, A., Nigg, E.A., and Silljé, H.H. (2006). Different Plk1 functions show distinct dependencies on Polo-Box domain-mediated targeting. Mol. Biol. Cell *17*, 448–459.

Hartwell, L.H., Mortimer, R.K., Culotti, J., and Culotti, M. (1973). Genetic control of the cell division cycle in yeast: V. genetic analysis of cdc mutants. Genetics *74*, 267–286.

Hauf, S., Cole, R.W., LaTerra, S., Zimmer, C., Schnapp, G., Walter, R., Heckel, A., van Meel, J., Rieder, C.L., and Peters, J.M. (2003). The small molecule Hesperadin reveals a role for Aurora B in correcting kinetochore-microtubule attachment and in maintaining the spindle assembly checkpoint. J. Cell Biol. *161*, 281–294.

Hegemann, B., Hutchins, J.R., Hudecz, O., Novatchkova, M., Rameseder, J., Sykora, M.M., Liu, S., Mazanek, M., Lénárt, P., Hériché, J.K., et al. (2011). Systematic phosphorylation analysis of human mitotic protein complexes. Sci. Signal. *4*, rs12.

Heinrich, S., Geissen, E.M., Kamenz, J., Trautmann, S., Widmer, C., Drewe, P., Knop, M., Radde, N., Hasenauer, J., and Hauf, S. (2013). Determinants of robustness in spindle assembly checkpoint signalling. Nat. Cell Biol. *15*, 1328–1339.

Hertz, E.P.T., Kruse, T., Davey, N.E., López-Méndez, B., Sigurðsson, J.O., Montoya, G., Olsen, J.V., and Nilsson, J. (2016). A conserved motif provides binding specificity to the PP2A-B56 phosphatase. Mol. Cell *63*, 686–695.

Hindriksen, S., Lens, S.M.A., and Hadders, M.A. (2017). The ins and outs of aurora B inner centromere localization. Front. Cell Dev. Biol. *5*, 112.

Hinshaw, S.M., and Harrison, S.C. (2019). The structure of the Ctf19c/CCAN from budding yeast. eLife *8*, e44239.

Hinshaw, S.M., Makrantoni, V., Harrison, S.C., and Marston, A.L. (2017). The kinetochore receptor for the cohesin loading complex. Cell *171*, 72–84.e13.

Holtrich, U., Wolf, G., Bräuninger, A., Karn, T., Böhme, B., Rübsamen-Waigmann, H., and Strebhardt, K. (1994). Induction and down-regulation of PLK, a human serine/threonine kinase expressed in proliferating cells and tumors. Proc. Natl. Acad. Sci. USA *91*, 1736–1740.

Hsu, J.Y., Sun, Z.W., Li, X., Reuben, M., Tatchell, K., Bishop, D.K., Grushcow, J.M., Brame, C.J., Caldwell, J.A., Hunt, D.F., et al. (2000). Mitotic phosphorylation of histone H3 is governed by Ipl1/aurora kinase and Glc7/PP1 phosphatase in budding yeast and nematodes. Cell *102*, 279–291.

Huang, H., Hittle, J., Zappacosta, F., Annan, R.S., Hershko, A., and Yen, T.J. (2008). Phosphorylation sites in BubR1 that regulate kinetochore attachment, tension, and mitotic exit. J. Cell Biol. *183*, 667–680.

Huis In 't Veld, P.J., Jeganathan, S., Petrovic, A., Singh, P., John, J., Krenn, V., Weissmann, F., Bange, T., and Musacchio, A. (2016). Molecular basis of outer kinetochore assembly on CENP-T. eLife *5*, e21007.

Ikeda, M., and Tanaka, K. (2017). Plk1 bound to Bub1 contributes to spindle assembly checkpoint activity during mitosis. Sci. Rep. *7*, 8794.

Ishida, T., and Kinoshita, K. (2007). PrDOS: prediction of disordered protein regions from amino acid sequence. Nucleic. Acids Res. W460–W464.

Jang, Y.J., Lin, C.Y., Ma, S., and Erikson, R.L. (2002a). Functional studies on the role of the C-terminal domain of mammalian polo-like kinase. Proc. Natl. Acad. Sci. USA *99*, 1984–1989.

Jang, Y.J., Ma, S., Terada, Y., and Erikson, R.L. (2002b). Phosphorylation of threonine 210 and the role of serine 137 in the regulation of mammalian polo-like kinase. J. Biol. Chem. *277*, 44115–44120.

Janicki, S.M., Tsukamoto, T., Salghetti, S.E., Tansey, W.P., Sachidanandam, R., Prasanth, K.V., Ried, T., Shav-Tal, Y., Bertrand, E., Singer, R.H., and Spector, D.L. (2004). From silencing to gene expression: real-time analysis in single cells. Cell *116*, 683–698.

Jia, L., Li, B., and Yu, H. (2016). The Bub1-Plk1 kinase complex promotes spindle checkpoint signalling through Cdc20 phosphorylation. Nat. Commun. *7*, 10818.

Jiang, H., He, X., Wang, S., Jia, J., Wan, Y., Wang, Y., Zeng, R., Yates, J., 3rd, Zhu, X., and Zheng, Y. (2014). A microtubule-associated zinc finger protein, BuGZ, regulates mitotic chromosome alignment by ensuring Bub3 stability and kinetochore targeting. Dev. Cell *28*, 268–281.

Johnson, T.M., Antrobus, R., and Johnson, L.N. (2008). Plk1 activation by Ste20-like kinase (Slk) phosphorylation and polo-box phosphopeptide binding assayed with the substrate translationally controlled tumor protein (TCTP). Biochemistry *47*, 3688–3696.

Joukov, V., and De Nicolo, A. (2018). Aurora-PLK1 cascades as key signaling modules in the regulation of mitosis. Sci. Signal. *11*, eaar4195.

Kaisari, S., Shomer, P., Ziv, T., Sitry-Shevah, D., Miniowitz-Shemtov, S., Teichner, A., and Hershko, A. (2019). Role of Polo-like kinase 1 in the regulation of the action of $p31^{comet}$ in the disassembly of mitotic checkpoint complexes. Proc. Natl. Acad. Sci. USA *116*, 11725–11730.

Kaitna, S., Mendoza, M., Jantsch-Plunger, V., and Glotzer, M. (2000). Incenp and an aurora-like kinase form a complex essential for chromosome segregation and efficient completion of cytokinesis. Curr. Biol. *10*, 1172–1181.

Kang, Y.H., Park, J.-E., Yu, L.-R., Soung, N.-K., Yun, S.-M., Bang, J.K., Seong, Y.-S., Yu, H., Garfield, S., Veenstra, T.D., and Lee, K.S. (2006). Self-regulated Plk1 recruitment to kinetochores by the Plk1-PBIP1 interaction is critical for proper chromosome segregation. Mol. Cell *24*, 409–422.

Kang, Y.H., Park, C.-H., Kim, T.-S., Soung, N.-K., Bang, J.K., Kim, B.Y., Park, J.-E., and Lee, K.S. (2011). Mammalian polo-like kinase 1-dependent regulation of the PBIP1-CENP-Q complex at kinetochores. J. Biol. Chem. *286*, 19744–19757.

Kelm, O., Wind, M., Lehmann, W.D., and Nigg, E.A. (2002). Cell cycle-regulated phosphorylation of the *Xenopus polo*-like kinase Plx1. J. Biol. Chem. *277*, 25247–25256.

Kettenbach, A.N., Schweppe, D.K., Faherty, B.K., Pechenick, D., Pletnev, A.A., and Gerber, S.A. (2011). Quantitative phosphoproteomics identifies substrates and functional modules of *Aurora* and *Polo*-like kinase activities in mitotic cells. Sci. Signal. *4*, rs5.

Kim, J.H., Shim, J., Ji, M.-J., Jung, Y., Bong, S.M., Jang, Y.-J., Yoon, E.K., Lee, S.J., Kim, K.G., Kim, Y.H., et al. (2014). The condensin component NCAPG2 regulates microtubule-kinetochore attachment through recruitment of Polo-like kinase 1 to kinetochores. Nat. Commun. *5*, 4588.

Kim, J., Ishiguro, K., Nambu, A., Akiyoshi, B., Yokobayashi, S., Kagami, A., Ishiguro, T., Pendas, A.M., Takeda, N., Sakakibara, Y., et al. (2015). Meikin is a conserved regulator of meiosis-I-specific kinetochore function. Nature *517*, 466–471.

Klare, K., Weir, J.R., Basilico, F., Zimniak, T., Massimiliano, L., Ludwigs, N., Herzog, F., and Musacchio, A. (2015). CENP-C is a blueprint for constitutive centromere-associated network assembly within human kinetochores. J. Cell Biol. *210*, 11–22.

Kothe, M., Kohls, D., Low, S., Coli, R., Cheng, A.C., Jacques, S.L., Johnson, T.L., Lewis, C., Loh, C., Nonomiya, J., et al. (2007). Structure of the catalytic domain of human polo-like kinase 1. Biochemistry *46*, 5960–5971.

Krenn, V., and Musacchio, A. (2015). The Aurora B kinase in chromosome bi-orientation and spindle checkpoint signaling. Front. Oncol. *5*, 225.

Krenn, V., Overlack, K., Primorac, I., van Gerwen, S., and Musacchio, A. (2014). KI motifs of human Knl1 enhance assembly of comprehensive spindle checkpoint complexes around MELT repeats. Curr. Biol. *24*, 29–39.

Kruse, T., Zhang, G., Larsen, M.S., Lischetti, T., Streicher, W., Kragh Nielsen, T., Bjørn, S.P., and Nilsson, J. (2013). Direct binding between BubR1 and B56-PP2A phosphatase complexes regulate mitotic progression. J. Cell Sci. *126*, 1086–1092.

Kumagai, A., and Dunphy, W.G. (1996). Purification and molecular cloning of Plx1, a Cdc25-regulatory kinase from Xenopus egg extracts. Science *273*, 1377–1380.

Lampson, M.A., and Grishchuk, E.L. (2017). Mechanisms to Avoid and Correct Erroneous Kinetochore-Microtubule Attachments. Biology (Basel) *6*, 1.

Lane, H.A., and Nigg, E.A. (1996). Antibody microinjection reveals an essential role for human polo-like kinase 1 (Plk1) in the functional maturation of mitotic centrosomes. J. Cell Biol. *135*, 1701–1713.

Laue, T.M., Shah, B.D., Ridgeway, T.M., and Pelletier, S.L. (1992). Analytical Ultracentrifugation in Biochemistry and Polymer Science (Royal Society of Chemistry), pp. 90–125.

Lee, K.S., Grenfell, T.Z., Yarm, F.R., and Erikson, R.L. (1998). Mutation of the polo-box disrupts localization and mitotic functions of the mammalian polo kinase Plk. Proc. Natl. Acad. Sci. USA *95*, 9301–9306.

Lee, K.S., Park, J.E., Kang, Y.H., Kim, T.S., and Bang, J.K. (2014). Mechanisms underlying Plk1 polo-box domain-mediated biological processes and their physiological significance. Mol. Cells *37*, 286–294.

Lee, H.-S., Park, Y.-Y., Cho, M.-Y., Chae, S., Yoo, Y.-S., Kwon, M.-H., Lee, C.-W., and Cho, H. (2015). The chromatin remodeller RSF1 is essential for PLK1 deposition and function at mitotic kinetochores. Nat. Commun. *6*, 7904.

Lénárt, P., Petronczki, M., Steegmaier, M., Di Fiore, B., Lipp, J.J., Hoffmann, M., Rettig, W.J., Kraut, N., and Peters, J.-M. (2007). The small-molecule inhibitor BI 2536 reveals novel insights into mitotic roles of polo-like kinase 1. Curr. Biol. *17*, 304–315.

Lera, R.F., Potts, G.K., Suzuki, A., Johnson, J.M., Salmon, E.D., Coon, J.J., and Burkard, M.E. (2016). Decoding Polo-like kinase 1 signaling along the kinetochore-centromere axis. Nat. Chem. Biol. *12*, 411–418.

Li, Y., Haarhuis, J.H.I., Sedeño Cacciatore, Á., Oldenkamp, R., van Ruiten, M.S., Willems, L., Teunissen, H., Muir, K.W., de Wit, E., Rowland, B.D., and Panne, D. (2020). The structural basis for cohesin-CTCF-anchored loops. Nature *578*, 472–476.

Liu, J., Lewellyn, A.L., Chen, L.G., and Maller, J.L. (2004). The polo box is required for multiple functions of Plx1 in mitosis. J. Biol. Chem. *279*, 21367–21373.

Liu, D., Vader, G., Vromans, M.J., Lampson, M.A., and Lens, S.M. (2009). Sensing chromosome bi-orientation by spatial separation of aurora B kinase from kinetochore substrates. Science *323*, 1350–1353.

Liu, D., Davydenko, O., and Lampson, M.A. (2012). Polo-like kinase-1 regulates kinetochore-microtubule dynamics and spindle checkpoint silencing. J. Cell Biol. *198*, 491–499.

Liu, H., Jia, L., and Yu, H. (2013). Phospho-H2A and cohesin specify distinct tension-regulated Sgo1 pools at kinetochores and inner centromeres. Curr. Biol. *23*, 1927–1933.

Llamazares, S., Moreira, A., Tavares, A., Girdham, C., Spruce, B.A., Gonzalez, C., Karess, R.E., Glover, D.M., and Sunkel, C.E. (1991). polo encodes a protein kinase homolog required for mitosis in Drosophila. Genes Dev. *5* (12A), 2153–2165.

Lobjois, V., Froment, C., Braud, E., Grimal, F., Burlet-Schiltz, O., Ducommun, B., and Bouche, J.P. (2011). Study of the docking-dependent PLK1 phosphorylation of the CDC25B phosphatase. Biochem. Biophys. Res. Commun. *410*, 87–90.

Lowery, D.M., Lim, D., and Yaffe, M.B. (2005). Structure and function of Polo-like kinases. Oncogene *24*, 248–259.

Lowery, D.M., Clauser, K.R., Hjerrild, M., Lim, D., Alexander, J., Kishi, K., Ong, S.E., Gammeltoft, S., Carr, S.A., and Yaffe, M.B. (2007). Proteomic screen defines the Polo-box domain interactome and identifies Rock2 as a Plk1 substrate. EMBO J. *26*, 2262–2273.

Lupas, A., Van Dyke, M., and Stock, J. (1991). Predicting coiled coils from protein sequences. Science *252*, 1162–1164.

Macůrek, L., Lindqvist, A., Lim, D., Lampson, M.A., Klompmaker, R., Freire, R., Clouin, C., Taylor, S.S., Yaffe, M.B., and Medema, R.H. (2008). Polo-like kinase-1 is activated by aurora A to promote checkpoint recovery. Nature *455*, 119–123.

Maia, A.R.R., Garcia, Z., Kabeche, L., Barisic, M., Maffini, S., Macedo-Ribeiro, S., Cheeseman, I.M., Compton, D.A., Kaverina, I., and Maiato, H. (2012). Cdk1 and Plk1 mediate a CLASP2 phospho-switch that stabilizes kinetochore-microtubule attachments. J. Cell Biol. *199*, 285–301.

Matsumura, S., Toyoshima, F., and Nishida, E. (2007). Polo-like kinase 1 facilitates chromosome alignment during prometaphase through BubR1. J. Biol. Chem. *282*, 15217–15227.

Matthess, Y., Raab, M., Knecht, R., Becker, S., and Strebhardt, K. (2014). Sequential Cdk1 and Plk1 phosphorylation of caspase-8 triggers apoptotic cell death during mitosis. Mol. Oncol. *8*, 596–608.

McKinley, K.L., and Cheeseman, I.M. (2014). Polo-like kinase 1 licenses CENP-A deposition at centromeres. Cell *158*, 397–411.

Michalski, A., Damoc, E., Hauschild, J.P., Lange, O., Wieghaus, A., Makarov, A., Nagaraj, N., Cox, J., Mann, M., and Horning, S. (2011). Mass spectrometry-based proteomics using Q Exactive, a high-performance benchtop quadrupole Orbitrap mass spectrometer. Mol. Cell Proteomics, 10, M111.011015.

Monda, J.K., and Cheeseman, I.M. (2018). The kinetochore-microtubule interface at a glance. J. Cell Sci. *131*, jcs214577.

Moriya, T., Saur, M., Stabrin, M., Merino, F., Voicu, H., Huang, Z., Penczek, P.A., Raunser, S., and Gatsogiannis, C. (2017). High-resolution Single Particle Analysis from Electron Cryo-microscopy Images Using SPHIRE. J. Vis. Exp. *123*, 55448.

Morrow, C.J., Tighe, A., Johnson, V.L., Scott, M.I., Ditchfield, C., and Taylor, S.S. (2005). Bub1 and aurora B cooperate to maintain BubR1-mediated inhibition of APC/CCdc20. J. Cell Sci. *118*, 3639–3652.

Moshe, Y., Boulaire, J., Pagano, M., and Hershko, A. (2004). Role of Polo-like kinase in the degradation of early mitotic inhibitor 1, a regulator of the anaphase promoting complex/cyclosome. Proc. Natl. Acad. Sci. USA *101*, 7937–7942.

Moutinho-Santos, T., Conde, C., and Sunkel, C.E. (2012). POLO ensures chromosome bi-orientation by preventing and correcting erroneous chromosome-spindle attachments. J. Cell Sci. *125*, 576–583.

Mulvihill, D.P., Petersen, J., Ohkura, H., Glover, D.M., and Hagan, I.M. (1999). Plo1 kinase recruitment to the spindle pole body and its role in cell division in Schizosaccharomyces pombe. Mol. Biol. Cell *10*, 2771–2785.

Mundt, K.E., Golsteyn, R.M., Lane, H.A., and Nigg, E.A. (1997). On the regulation and function of human polo-like kinase 1 (PLK1): effects of overexpression on cell cycle progression. Biochem. Biophys. Res. Commun. *239*, 377–385.

Musacchio, A., and Desai, A. (2017). A molecular view of kinetochore assembly and function. Biology (Basel) *6*, 5.

Nakajima, H., Toyoshima-Morimoto, F., Taniguchi, E., and Nishida, E. (2003). Identification of a consensus motif for Plk (Polo-like kinase) phosphorylation reveals Myt1 as a Plk1 substrate. J. Biol. Chem. *278*, 25277–25280.

Natsume, T., Müller, C.A., Katou, Y., Retkute, R., Gierliński, M., Araki, H., Blow, J.J., Shirahige, K., Nieduszynski, C.A., and Tanaka, T.U. (2013). Kinetochores coordinate pericentromeric cohesion and early DNA replication by Cdc7-Dbf4 kinase recruitment. Mol. Cell *50*, 661–674.

Neef, R., Preisinger, C., Sutcliffe, J., Kopajtich, R., Nigg, E.A., Mayer, T.U., and Barr, F.A. (2003). Phosphorylation of mitotic kinesin-like protein 2 by polo-like kinase 1 is required for cytokinesis. J. Cell Biol. *162*, 863–875.

Neef, R., Gruneberg, U., Kopajtich, R., Li, X., Nigg, E.A., Sillje, H., and Barr, F.A. (2007). Choice of Plk1 docking partners during mitosis and cytokinesis is controlled by the activation state of Cdk1. Nat. Cell Biol. *9*, 436–444.

Nezi, L., and Musacchio, A. (2009). Sister chromatid tension and the spindle assembly checkpoint. Curr. Opin. Cell Biol. *21*, 785–795.

Nishino, M., Kurasawa, Y., Evans, R., Lin, S.-H., Brinkley, B.R., and Yu-Lee, L.Y. (2006). NudC is required for Plk1 targeting to the kinetochore and chromosome congression. Curr. Biol. *16*, 1414–1421.

Novak, B., Kapuy, O., Domingo-Sananes, M.R., and Tyson, J.J. (2010). Regulated protein kinases and phosphatases in cell cycle decisions. Curr. Opin. Cell Biol. *22*, 801–808.

O'Connor, A., Maffini, S., Rainey, M.D., Kaczmarczyk, A., Gaboriau, D., Musacchio, A., and Santocanale, C. (2015). Requirement for PLK1 kinase activity in the maintenance of a robust spindle assembly checkpoint. Biol. Open *5*, 11–19.

O'Donovan, D.S., MacFhearraigh, S., Whitfield, J., Swigart, L.B., Evan, G.I., and Mc Gee, M.M. (2013). Sequential Cdk1 and Plk1 phosphorylation of protein tyrosine phosphatase 1B promotes mitotic cell death. Cell Death Dis. *4*, e468.

Ohkura, H., Hagan, I.M., and Glover, D.M. (1995). The conserved Schizosaccharomyces pombe kinase plo1, required to form a bipolar spindle, the actin ring, and septum, can drive septum formation in G1 and G2 cells. Genes Dev. *9*, 1059–1073.

Olsen, J.V., Macek, B., Lange, O., Makarov, A., Horning, S., and Mann, M. (2007). Higher-energy C-trap dissociation for peptide modification analysis. Nat. Methods *4*, 709–712.

Overlack, K., Primorac, I., Vleugel, M., Krenn, V., Maffini, S., Hoffmann, I., Kops, G.J., and Musacchio, A. (2015). A molecular basis for the differential roles of Bub1 and BubR1 in the spindle assembly checkpoint. eLife *4*, e05269.

Pan, D., Klare, K., Petrovic, A., Take, A., Walstein, K., Singh, P., Rondelet, A., Bird, A.W., and Musacchio, A. (2017). CDK-regulated dimerization of M18BP1 on a Mis18 hexamer is necessary for CENP-A loading. eLife *6*, e23352.

Park, J.E., Soung, N.K., Johmura, Y., Kang, Y.H., Liao, C., Lee, K.H., Park, C.H., Nicklaus, M.C., and Lee, K.S. (2010). Polo-box domain: a versatile mediator of polo-like kinase function. Cell. Mol. Life Sci. *67*, 1957–1970.

Pentakota, S., Zhou, K., Smith, C., Maffini, S., Petrovic, A., Morgan, G.P., Weir, J.R., Vetter, I.R., Musacchio, A., and Luger, K. (2017). Decoding the centromeric nucleosome through CENP-N. eLife *6*, e33442.

Pesenti, M.E., Prumbaum, D., Auckland, P., Smith, C.M., Faesen, A.C., Petrovic, A., Erent, M., Maffini, S., Pentakota, S., Weir, J.R., et al. (2018). Reconstitution of a 26-subunit human kinetochore reveals cooperative microtubule binding by CENP-OPQUR and NDC80. Mol. Cell *71*, 923–939.e910.

Peters, U., Cherian, J., Kim, J.H., Kwok, B.H., and Kapoor, T.M. (2006). Probing cell-division phenotype space and Polo-like kinase function using small molecules. Nat. Chem. Biol. *2*, 618–626.

Petrovic, A., Pasqualato, S., Dube, P., Krenn, V., Santaguida, S., Cittaro, D., Monzani, S., Massimiliano, L., Keller, J., Tarricone, A., et al. (2010). The MIS12 complex is a protein interaction hub for outer kinetochore assembly. J. Cell Biol. *190*, 835–852.

Petrovic, A., Mosalaganti, S., Keller, J., Mattiuzzo, M., Overlack, K., Krenn, V., De Antoni, A., Wohlgemuth, S., Cecatiello, V., Pasqualato, S., et al. (2014). Modular assembly of RWD domains on the Mis12 complex underlies outer kinetochore organization. Mol. Cell *53*, 591–605.

Pettersen, E.F., Goddard, T.D., Huang, C.C., Couch, G.S., Greenblatt, D.M., Meng, E.C., and Ferrin, T.E. (2004). UCSF Chimera--a visualization system for exploratory research and analysis. J. Comput. Chem. *25*, 1605–1612.

Porter, I.M., Schleicher, K., Porter, M., and Swedlow, J.R. (2013). Bod1 regulates protein phosphatase 2A at mitotic kinetochores. Nat. Commun. *4*, 2677.

Pouwels, J., Kukkonen, A.M., Lan, W., Daum, J.R., Gorbsky, G.J., Stukenberg, T., and Kallio, M.J. (2007). Shugoshin 1 plays a central role in kinetochore assembly and is required for kinetochore targeting of Plk1. Cell Cycle *6*, 1579–1585.

Qi, W., Tang, Z., and Yu, H. (2006). Phosphorylation- and polo-box-dependent binding of Plk1 to Bub1 is required for the kinetochore localization of Plk1. Mol. Biol. Cell *17*, 3705–3716.

Rago, F., and Cheeseman, I.M. (2013). Review series: the functions and consequences of force at kinetochores. J. Cell Biol. *200*, 557–565.

Rappsilber, J., Mann, M., and Ishihama, Y. (2007). Protocol for micro-purification, enrichment, pre-fractionation and storage of peptides for proteomics using StageTips. Nat. Protoc. *2*, 1896–1906.

Santaguida, S., Tighe, A., D'Alise, A.M., Taylor, S.S., and Musacchio, A. (2010). Dissecting the role of MPS1 in chromosome biorientation and the spindle checkpoint through the small molecule inhibitor reversine. J. Cell Biol. *190*, 73–87.

Saurin, A.T. (2018). Kinase and phosphatase cross-talk at the kinetochore. Front. Cell Dev. Biol. *6*, 62.

Schindelin, J., Arganda-Carreras, I., Frise, E., Kaynig, V., Longair, M., Pietzsch, T., Preibisch, S., Rueden, C., Saalfeld, S., Schmid, B., et al. (2012). Fiji: an open-source platform for biological-image analysis. Nat. Methods *9*, 676–682.

Schuck, P. (2000). Size-distribution analysis of macromolecules by sedimentation velocity ultracentrifugation and lamm equation modeling. Biophys. J. *78*, 1606–1619.

Seki, A., Coppinger, J.A., Jang, C.Y., Yates, J.R., and Fang, G. (2008). Bora and the kinase Aurora a cooperatively activate the kinase Plk1 and control mitotic entry. Science *320*, 1655–1658.

Seong, Y.S., Kamijo, K., Lee, J.S., Fernandez, E., Kuriyama, R., Miki, T., and Lee, K.S. (2002). A spindle checkpoint arrest and a cytokinesis failure by the dominant-negative polo-box domain of Plk1 in U-2 OS cells. J. Biol. Chem. *277*, 32282–32293.

Sessa, F., Mapelli, M., Ciferri, C., Tarricone, C., Areces, L.B., Schneider, T.R., Stukenberg, P.T., and Musacchio, A. (2005). Mechanism of Aurora B activation by INCENP and inhibition by hesperadin. Mol. Cell *18*, 379–391.

Shao, H., Huang, Y., Zhang, L., Yuan, K., Chu, Y., Dou, Z., Jin, C., Garcia-Barrio, M., Liu, X., and Yao, X. (2015). Spatiotemporal dynamics of Aurora B-PLK1-MCAK signaling axis orchestrates kinetochore bi-orientation and faithful chromosome segregation. Sci. Rep. *5*, 12204.

Songyang, Z., Lu, K.P., Kwon, Y.T., Tsai, L.H., Filhol, O., Cochet, C., Brickey, D.A., Soderling, T.R., Bartleson, C., Graves, D.J., et al. (1996). A structural basis for substrate specificities of protein Ser/Thr kinases: primary sequence preference of casein kinases I and II, NIMA, phosphorylase kinase, calmodulin-dependent kinase II, CDK5, and Erk1. Mol. Cell. Biol. *16*, 6486–6493.

Suijkerbuijk, S.J., van Dam, T.J., Karagöz, G.E., von Castelmur, E., Hubner, N.C., Duarte, A.M., Vleugel, M., Perrakis, A., Rüdiger, S.G., Snel, B., and Kops, G.J. (2012a). The vertebrate mitotic checkpoint protein BUBR1 is an unusual pseudokinase. Dev. Cell *22*, 1321–1329.

Suijkerbuijk, S.J., Vleugel, M., Teixeira, A., and Kops, G.J. (2012b). Integration of kinase and phosphatase activities by BUBR1 ensures formation of stable kinetochore-microtubule attachments. Dev. Cell *23*, 745–755.

Sun, S.-C., Liu, H.-L., and Sun, Q.-Y. (2012). Survivin regulates Plk1 localization to kinetochore in mouse oocyte meiosis. Biochem. Biophys. Res. Commun. *421*, 797–800.

Sunkel, C.E., and Glover, D.M. (1988). polo, a mitotic mutant of *Drosophila* displaying abnormal spindle poles. J. Cell Sci. *89*, 25–38.

Tighe, A., Staples, O., and Taylor, S. (2008). Mps1 kinase activity restrains anaphase during an unperturbed mitosis and targets Mad2 to kinetochores. J. Cell Biol. *181*, 893–901.

Ubersax, J.A., and Ferrell, J.E., Jr. (2007). Mechanisms of specificity in protein phosphorylation. Nat. Rev. Mol. Cell Biol. *8*, 530–541.

van der Waal, M.S., Saurin, A.T., Vromans, M.J., Vleugel, M., Wurzenberger, C., Gerlich, D.W., Medema, R.H., Kops, G.J., and Lens, S.M. (2012). Mps1 promotes rapid centromere accumulation of Aurora B. EMBO Rep. *13*, 847–854.

Vassilev, L.T., Tovar, C., Chen, S., Knezevic, D., Zhao, X., Sun, H., Heimbrook, D.C., and Chen, L. (2006). Selective small-molecule inhibitor reveals critical mitotic functions of human CDK1. Proc. Natl. Acad. Sci. USA *103*, 10660–10665.

Vleugel, M., Tromer, E., Omerzu, M., Groenewold, V., Nijenhuis, W., Snel, B., and Kops, G.J. (2013). Arrayed BUB recruitment modules in the kinetochore scaffold KNL1 promote accurate chromosome segregation. J. Cell Biol. *203*, 943–955.

von Schubert, C., Cubizolles, F., Bracher, J.M., Sliedrecht, T., Kops, G.J.P.L., and Nigg, E.A. (2015). Plk1 and Mps1 cooperatively regulate the spindle assembly checkpoint in human cells. Cell Rep. *12*, 66–78.

Wang, F., Ulyanova, N.P., van der Waal, M.S., Patnaik, D., Lens, S.M.A., and Higgins, J.M.G. (2011). A positive feedback loop involving Haspin and Aurora B promotes CPC accumulation at centromeres in mitosis. Curr. Biol. *21*, 1061–1069.

Watanabe, N., Arai, H., Nishihara, Y., Taniguchi, M., Watanabe, N., Hunter, T., and Osada, H. (2004). M-phase kinases induce phospho-dependent ubiquitination of somatic Wee1 by SCFbeta-TrCP. Proc. Natl. Acad. Sci. USA *101*, 4419–4424.

Weir, J.R., Faesen, A.C., Klare, K., Petrovic, A., Basilico, F., Fischböck, J., Pentakota, S., Keller, J., Pesenti, M.E., Pan, D., et al. (2016). Insights from biochemical reconstitution into the architecture of human kinetochores. Nature *537*, 249–253.

Weissmann, F., Petzold, G., VanderLinden, R., Huis In 't Veld, P.J., Brown, N.G., Lampert, F., Westermann, S., Stark, H., Schulman, B.A., and Peters, J.M. (2016). biGBac enables rapid gene assembly for the expression of large multisubunit protein complexes. Proc. Natl. Acad. Sci. USA *113*, E2564–E2569.

Wimbish, R.T., and DeLuca, J.G. (2020). Hec1/Ndc80 tail domain function at the kinetochore-microtubule interface. Front. Cell Dev. Biol. *8*, 43.

Wolfe, B.A., Takaki, T., Petronczki, M., and Glotzer, M. (2009). Polo-like kinase 1 directs assembly of the HsCyk-4 RhoGAP/Ect2 RhoGEF complex to initiate cleavage furrow formation. PLoS Biol. *7*, e1000110.

Wong, O.K., and Fang, G. (2007). Cdk1 phosphorylation of BubR1 controls spindle checkpoint arrest and Plk1-mediated formation of the 3F3/2 epitope. J. Cell Biol. *179*, 611–617.

Xu, J., Shen, C., Wang, T., and Quan, J. (2013). Structural basis for the inhibition of Polo-like kinase 1. Nat. Struct. Mol. Biol. *20*, 1047–1053.

Yamaguchi, T., Goto, H., Yokoyama, T., Silljé, H., Hanisch, A., Uldschmid, A., Takai, Y., Oguri, T., Nigg, E.A., and Inagaki, M. (2005). Phosphorylation by Cdk1 induces Plk1-mediated vimentin phosphorylation during mitosis. J. Cell Biol. *171*, 431–436.

Yamashiro, S., Yamakita, Y., Totsukawa, G., Goto, H., Kaibuchi, K., Ito, M., Hartshorne, D.J., and Matsumura, F. (2008). Myosin phosphatase-targeting subunit 1 regulates mitosis by antagonizing polo-like kinase 1. Dev. Cell *14*, 787–797.

Yan, K., Yang, J., Zhang, Z., McLaughlin, S.H., Chang, L., Fasci, D., Ehrenhofer-Murray, A.E., Heck, A.J.R., and Barford, D. (2019). Structure of the inner kinetochore CCAN complex assembled onto a centromeric nucleosome. Nature *574*, 278–282.

Yeh, T.Y., Kowalska, A.K., Scipioni, B.R., Cheong, F.K., Zheng, M., Derewenda, U., Derewenda, Z.S., and Schroer, T.A. (2013). Dynactin helps target Polo-like kinase 1 to kinetochores via its left-handed beta-helical p27 subunit. EMBO J. *32*, 1023–1035.

Yoo, H.Y., Kumagai, A., Shevchenko, A., Shevchenko, A., and Dunphy, W.G. (2004). Adaptation of a DNA replication checkpoint response depends upon inactivation of Claspin by the Polo-like kinase. Cell *117*, 575–588.

Zhang, X., Chen, Q., Feng, J., Hou, J., Yang, F., Liu, J., Jiang, Q., and Zhang, C. (2009). Sequential phosphorylation of Nedd1 by Cdk1 and Plk1 is required for targeting of the gammaTuRC to the centrosome. J. Cell Sci. *122*, 2240–2251.

Zhou, H., Di Palma, S., Preisinger, C., Peng, M., Polat, A.N., Heck, A.J., and Mohammed, S. (2013). Toward a comprehensive characterization of a human cancer cell phosphoproteome. J. Proteome Res. *12*, 260–271.

Zhu, K., Shan, Z., Zhang, L., and Wen, W. (2016). Phospho-pon binding-mediated fine-tuning of Plk1 activity. Structure *24*, 1110–1119.

Zhuo, X., Guo, X., Zhang, X., Jing, G., Wang, Y., Chen, Q., Jiang, Q., Liu, J., and Zhang, C. (2015). Usp16 regulates kinetochore localization of Plk1 to promote proper chromosome alignment in mitosis. J. Cell Biol. *210*, 727–735.

Zitouni, S., Nabais, C., Jana, S.C., Guerrero, A., and Bettencourt-Dias, M. (2014). Polo-like kinases: structural variations lead to multiple functions. Nat. Rev. Mol. Cell Biol. *15*, 433–452.

## STAR★METHODS

### KEY RESOURCES TABLE

| REAGENT or RESOURCE | SOURCE | IDENTIFIER |
|---|---|---|
| Antibodies | | |
| anti-Mps1 rabbit polyclonal | This study | 933 Affinity purified |
| anti-CENP-O rabbit polyclonal | Amaro et al., 2010 | NA |
| anti-Tubulin mouse monoclonal | Sigma | Cat#T9026; RRID: AB_477593 |
| anti-GFP rabbit polyclonal | Abcam | Cat#ab190584 |
| anti-BubR1 mouse monoclonal | BD | Cat#612503; RRID: AB_2066085 |
| anti-Incenp rabbit polyclonal | Cell Signaling | Cat#2807; RRID: AB_2127513 |
| anti-Plk1 mouse monoclonal | Abcam | Cat#ab17057; RRID: AB_443613 |
| anti-Cyclin B mouse monoclonal | Santa Cruz | Cat#Sc-245; RRID: AB_627338 |
| anti-Vinculin mouse monoclonal | Sigma | Cat#V9131; RRID: AB_477629 |
| anti-Aurora B mouse monoclonal | Abcam | Cat#ab3609; RRID: AB_449204 |
| anti-BUB1 rabbit polyclonal | Abcam | Cat#ab9000; RRID: AB_449765 |
| anti-BUBR1 rabbit polyclonal | Abcam | Cat#ab70544; RRID: AB_1209397 |
| anti-mouse IgG-Alexa 488 secondary | Invitrogen | Cat#A11001; RRID: AB_2534069 |
| anti-rabbit IgG-Alexa 488 secondary | Invitrogen | Cat#A21206; RRID: AB_2535792 |
| anti-mouse IgG-Rhodamine secondary | Jackson Imm.Res | Cat#115-295-003; RRID: AB_2338756 |
| anti-rabbit IgG- Rhodamine secondary | Jackson Imm.Res | Cat#111-295-003; RRID: AB_2338022 |
| anti-human IgG-Alexa 647 secondary | Invitrogen | Cat#A21445; RRID: AB_2535862 |
| Human anti-centromere (CREST) | Antibodies Inc. | Cat#15-234-0001; RRID: AB_2687472 |
| anti-H3pS10 rabbit polyclonal | Abcam | Cat#ab5176; RRID: AB_304763 |
| anti-Cep135 rabbit | Bird and Hyman, 2008 | N/A |
| anti-CENP-QU goat polyclonal | Pesenti et al., 2018 | N/A |
| anti-pT232 Aurora B rabbit polyclonal | Rockland | Cat#660-401-677; RRID: AB_2061641 |
| anti-H2ApT120 rabbit polyclonal | Active Motif | Cat#39391; RRID: AB_2744670 |
| Goat anti-rabbit DyLight 405 | Jackson Immuno Research | Cat#111-475-003; RRID: AB_2338035 |
| Donkey anti-goat 488 | Invitrogen | Cat#A11055; RRID: AB_2534102 |
| Chicken anti-rabbit Alexa Fluor 647 | Invitrogen | Cat#A11046; RRID: AB_142716 |
| Bacterial and Virus Strains | | |
| E.coli: BL21(DE3)-RIL strain | Agilent Technologies | Cat#230240 |
| E.coli: BL21CodonPlus(DE3)-RIL strain | Agilent Technologies | Cat#230280 |
| *E. coli* BL21 (DH5α) | ThermoFisher | Cat#18265017 |
| Insect Cells | | |
| S.frugiperda:Sf9 cells | ThermoFisher | Cat#12659017 |
| Trichoplusia ni:BTI-Tnao38 | Garry W Blissard Lab | N/A |
| Chemicals, Peptides, and Recombinant Proteins | | |
| Okadaic Acid | Merck | Cat#04906845001 |
| RO-3306 | Millipore | Cat#217699 |
| MG-132 | Calbiochem | CAS 133407-82-6 |
| Reversine | Cayman Chemical | Cat#10004412 |
| Hesperadin | Merck | Cat#375680-5MG |
| Fetal bovine serum (FBS) | Clonetech | Cat#631107 |
| Zeocin | Invitrogen | Cat#R25001 |
| L-glutamine | PAN Biotech | Cat#P04-80100 |
| Nocodazole | Sigma | Cat#M1404 |

(*Continued on next page*)

*Continued*

| REAGENT or RESOURCE | SOURCE | IDENTIFIER |
|---|---|---|
| RNAiMAX | Invitrogen | Cat#13778100 |
| DAPI | Sigma | Cat#D9542 |
| PenStrep | GIBCO | Cat#15-140 |
| Oligofectamine | Invitrogen | Cat#12252011 |
| Thymidine | Sigma | Cat#T9250 |
| Trypsin EDTA | PAN | Cat#P10-027100 |
| Doxycycline | Sigma | Cat#D9891 |
| Triton-100 | Sigma | Cat#T8787 |
| Paraformaldehyde | VWR | Cat#100503-914 |
| NEON transfection Kit (includes buffers) | Invitrogen | Cat#MPK10096 |
| PhosSTOP phosphatase inhibitor | Roche | Cat#4906845001 |
| Alexa Fluor 488 C5 maleimide Protein labeling kit | ThermoFisher | Cat#A10254 |
| Blasticidin | Invitrogen | Cat#A1113902 |
| Hygromycin B | Invitrogen | Cat#10687010 |
| DMEM | PAN Biotech | Cat#P0403609 |
| Fetal Bovine Serum (FBS) | PAN Biotech | Cat#P303031 |
| Penicillin/Streptomycin | PAN Biotech | Cat#P0607300 |
| Lipofectamine 2000 | Invitrogen | Cat#11668019 |
| Oligofectamine | Thermo Fischer | Cat#12252011 |
| X-tremeGENE | Roche | Cat#4476093001 |
| BI2536 | Selleck | Cat#S1109 |
| Poly-D-Lysine | Sigma-Aldrich | Cat#A003E |
| PIPES | Sigma-Aldrich | Cat#P6757 |
| HEPES | Sigma-Aldrich | Cat#H3375 |
| EGTA | Sigma-Aldrich | Cat#324626 |
| $MgCl_2$ | Sigma-Aldrich | Cat#M8266 |
| BSA | Sigma-Aldrich | Cat#B6917 |
| Mowiol | Calbiochem | Cat#475904 |
| IPTG | Sigma-Aldrich | Cat#I6758 |
| NaCl | Sigma-Aldrich | Cat#S9888 |
| Glycerol | Sigma-Aldrich | Cat#G5516 |
| Imidazole | Sigma-Aldrich | Cat#I5513 |
| TCEP | Sigma-Aldrich | Cat#75259 |
| Protease Inhibitor Cocktail | Serva | Cat#39107 |
| HiTrap TALON crude | GE Healthcare | Cat#45-002-386 |
| Glutathione Sepharose 4 Fast Flow beads | GE Healthcare | Cat#17-5132-01 |
| Resource Q anion exchange chromatography column | GE Healthcare | Cat#17-1179-01 |
| L-reduced Glutathione | Sigma-Aldrich | Cat#G6529 |
| Pro-Q Diamond phosphoprotein stain | Thermo Fischer | Cat#P33300 |
| Coomassie Brilliant Blue R-250 dye | Thermo Fischer | Cat#20278 |
| Alexa Fluor 488 C5 maleimide Protein labeling kit | Thermo Fischer | Cat#A10254 |
| CENP-OPQUR complex | Pesenti et al., 2018 | N/A |
| CENP-QU complex | Pesenti et al., 2018 | N/A |
| CENP-OP complex | Pesenti et al., 2018 | N/A |
| CENP-LN complex | Pentakota et al., 2017 | N/A |
| CENP-CHKIM complex | Weir et al., 2016 | N/A |
| MIS12 complex | Petrovic et al., 2014 | N/A |
| NDC80 complex | Huis In 't Veld et al., 2016 | N/A |

(*Continued on next page*)

*Continued*

| REAGENT or RESOURCE | SOURCE | IDENTIFIER |
|---|---|---|
| KNL1 complex | Petrovic et al., 2014 | N/A |
| BUB1:BUB3 complex | Breit et al., 2015 | N/A |
| BUBR1:BUB3 complex | Breit et al., 2015 | N/A |
| BUB1 kinase (BUB1$^{705-1050}$) | Breit et al., 2015 | N/A |
| Aurora B kinase (Aurora B$^{45-344}$:INCENP$^{835-903}$) | Girdler et al., 2008 | N/A |
| PLK1 kinase | Pan et al., 2017 | N/A |
| CDK1 kinase (CDK1:CyclinB complex) | This study | N/A |
| MPS1 kinase | This study | N/A |
| CENP-OPQU$^{114-418}$R | This study | N/A |
| PLK1$^{210A}$ | This study | N/A |
| PLK1$^{PBD}$ | This study | N/A |
| CENP-U$^{58-114}$ | This study | N/A |
| CENP-U$^{58-114}$T98A | This study | N/A |
| CENP-U$^{58-114}$S77A/T78A | This study | N/A |
| Deposited Data | | |
| Proteomics data | This study | PXD: 022033 |
| Unprocessed images | This study | https://doi.org/10.17632/rhgb7xcv5c.1 |
| Experimental Models: Cell Lines | | |
| HeLa cells | IEO Milan | N/A |
| U2OS-LacO | Janicki et al., 2004 | N/A |
| HeLa Flp-In T-REx | Tighe et al., 2008 | N/A |
| HeLa Flp-In T-REx_CENP-B-INCENP-EGFP | This study | N/A |
| HeLa Flp-In T-REx_EGFP-CENP-U_1-418 | This study | N/A |
| HeLa Flp-In T-REx_EGFP-CENP-U_1-114 | This study | N/A |
| HeLa Flp-In T-REx _EGFP-CENP-U_115-418 | This study | N/A |
| HeLa Flp-In T-REx_EGFP-CENP-U_S77/78A | This study | N/A |
| HeLa Flp-In T-REx_EGFP-CENP-U_T98A | This study | N/A |
| Oligonucleotides | | |
| CENP-Q smart pool | Dharmacon/Horizon | Cat#L-020768-02 |
| CENP-Q | Amaro et al., 2010 | N/A |
| CENP-U smart pool | Dharmacon/Horizon | Cat#L-004988-00 |
| CENP-O | Dharmacon/Horizon | Cat#L-014339-02-0005 |
| CENP-P | Amaro et al., 2010 | N/A |
| Bub1 #2 | Overlack et al., 2015 | N/A |
| BubR1_NEW176-196 | Overlack et al., 2015 | N/A |
| Recombinant DNA | | |
| pCDNA5/FRT/TO | Invitrogen | Cat#V601020 |
| pCDNA5/FRT/TO-EGFP-IRES | Petrovic et al., 2010 | N/A |
| pCDNA5/FRT/TO-EGFP-IRES_EGFP-CENP-U_1-418 | This study | N/A |
| pCDNA5/FRT/TO-EGFP-IRES_EGFP-CENP-U_1-114 | This study | N/A |
| pCDNA5/FRT/TO-EGFP-IRES_EGFP-CENP-U_115-418 | This study | N/A |
| pCDNA5/FRT/TO-EGFP-IRES_EGFP-CENP-U_S77/78A | This study | N/A |
| pCDNA5/FRT/TO-EGFP-IRES_EGFP-CENP-U_T98A | This study | N/A |
| LacI-EGFP | This study | N/A |
| Lac-I-EGFP-CENP-U_1-418 | This study | N/A |
| Lac-I-EGFP-CENP-U_1-114 | This study | N/A |
| Lac-I-EGFP-CENP-U_115-418 | This study | N/A |
| Lac-I-EGFP-CENP-U_1-57 | This study | N/A |

(*Continued on next page*)

*Continued*

| REAGENT or RESOURCE | SOURCE | IDENTIFIER |
|---|---|---|
| Lac-I-EGFP-CENP-U_58-114 | This study | N/A |
| Lac-I-EGFP-CENP-U_86-114 | This study | N/A |
| Lac-I-EGFP-CENP-U_58-85 | This study | N/A |
| pCDNA5/FRT/TO-EGFP-IRES_CENP-B-INCENP-EGFP | De Antoni et al., 2012 | N/A |
| pETDuet-1 | Novagen | Cat#71146 |
| pETDuet-1_6xHis-MBP-PLK1_PBD | This study | N/A |
| pETDuet-1_6xHis-MBP-PLK1_T210A | This study | N/A |
| pETDuet-1_6xHis-MBP-CENP-U$^{58-114}$ | This study | N/A |
| pETDuet-1_6xHis-MBP-CENP- U$^{58-114}$_S77A/T78A | This study | N/A |
| pETDuet-1_6xHis-MBP-CENP- U$^{58-114}$_T98A | This study | N/A |
| pLIB | Addgene | Cat#80610 |
| pLIB_6xHis_PLK1 | Pan et al., 2017 | N/A |
| pLIB_GST-CDK1 | This study | N/A |
| pLIB_6xHis-Cyclin B1 | This study | N/A |
| pBIGa | Addgene | Cat#80611 |
| pBIGa_GST-CDK1_6xHis-CyclinB1 | This study | N/A |
| pBIGa_CENP-O_P_6xHisQ_U_R | Pesenti et al., 2018 | N/A |
| pBIGa_CENP-O_P_6xHisQ_U$^{114-418}$_R | This study | N/A |
| pBIGa_6xHis-CENP-C$^{1-544}$_H_K_I$^{57-C}$_M | Weir et al., 2016 | N/A |
| pBIGa_NDC80_NUF2_6xHis-SPC25_SPC24 | Huis In 't Veld et al., 2016 | N/A |
| pLIB_GST-MPS1 | This study | N/A |
| pFL Multibac | Geneva Biotech | N/A |
| pFL_6xHis-BUB1$^{705-1050}$ | Breit et al., 2015 | N/A |
| pFL_6xHis-BUB1_BUB3 | Breit et al., 2015 | N/A |
| pFL_6xHis-BUBR1_BUB3 | Breit et al., 2015 | N/A |
| pFL_6xHis-CENP-Q-U | Pesenti et al., 2018 | N/A |
| pFL_6xHis-CENP-O-P | Pesenti et al., 2018 | N/A |
| pFL_GST-CENP-L_CENP-N | Pentakota et al., 2017 | N/A |
| pFL_DSN1-6xHis_NSL1 | Petrovic et al., 2014 | N/A |
| pFL_NNF1-MIS12 | Petrovic et al., 2014 | N/A |
| pGEX-6P | GE Healthcare | Cat#27-4598-01 |
| pGEX-6P-2rbs_GST-Aurora B$^{45-344}$:INCENP$^{835-903}$ | Girdler et al., 2008 | N/A |
| pGEX-6P-2rbs_GST-KNL1$^{1995-2316}$ | Petrovic et al., 2010 | N/A |
| pGEX-6P-2rbs-GST-ZWINT | Petrovic et al., 2010 | N/A |
| Software and Algorithms | | |
| GraphPad Prism 6.0 | GraphPad software | https://www.graphpad.com |
| Imaris 9.2 | Bitplane | https://imaris.oxinst.com/packages |
| ImageJ 1.46/ Fiji | NIH | https://imageJ.nih.gov/ij/ |
| SoftWorx | Applied Precision | N/A |
| Slidebook 6.0 | 3i | N/A |
| Image Lab | Bio-rad | https://www.bio-rad.com/de-de/product/image-lab-software?ID=KRE6P5E8Z |
| UCSF Chimera | Pettersen et al., 2004 | http://www.cgl.ucsf.edu/chimera |
| SPHIRE suit | Moriya et al., 2017 | http://www.sphire.mpg.de |
| SEDFIT | Schuck, 2000 | http://www.analyticalultracentrifugation.com/default.htm |
| SEDNTERP | Laue et al., 1992 | http://bitcwiki.sr.unh.edu/index.php/Main_Page |

(*Continued on next page*)

*Continued*

| REAGENT or RESOURCE | SOURCE | IDENTIFIER |
|---|---|---|
| GUSSI | Chad Brautigam | https://www.utsouthwestern.edu/labs/mbr/software/ |
| PrDOS | Ishida and Kinoshita, 2007 | http://prdos.hgc.jp/cgi-bin/top.cgi |
| COILS | Lupas et al., 1991 | https://embnet.vital-it.ch/software/COILS_form.html |
| Image Lab software Version 5.2 | Biorad | https://www.bio-rad.com/de-de/product/image-lab-software?ID=KRE6P5E8Z |

## RESOURCE AVAILABILITY

### Lead Contact

Requests for resources and reagents should be directed to the Lead Contact, Andrea Musacchio (andrea.musacchio@mpi-dortmund.mpg.de).

### Materials Availability

The plasmids and cell lines generated in this study are available on request to the Lead Contact.

### Data and Code Availability

Proteomics data have been deposited to the ProteomeXchange Consortium via the PRIDE partner repository with dataset identifier PXD: 022033. All the original/source data for Figures 1, 2, 3, 4, 5, 6, and S1–S7 are available on Mendeley (Mendeley Data: https://doi.org/10.17632/rhgb7xcv5c.1).

## EXPERIMENTAL MODEL AND SUBJECT DETAILS

### Cells lines and Expression strains

HeLa and U2OS-LacO (a gift by Geert Kops, UMC, Utrecht, Netherlands; (Janicki et al., 2004)) cell lines were maintained in DMEM (PAN Biotech, Aidenbach, Germany) supplemented with 10% FBS (PAN Biotech), 50 μg/ml Penicillin/Streptomycin (PAN Biotech), and 2 mM L-glutamine (PAN Biotech). HeLa Flp-In T-REx host cell lines (Tighe et al., 2008) were maintained in complete DMEM media as described above, but containing 10% tetracycline-free FBS (PAN Biotech) instead and supplemented with 50 μg/ml Zeocin (Invitrogen, Carlsbad, California, United States). Flp-In T-REx HeLa cells expressing GFP-fusions were generated as previously described (Tighe et al., 2008), maintained in DMEM with 10% tetracycline-free FBS supplemented with 250 μg/ml hygromycin and 4 μg/ml blastidicin (Invitrogen, Carlsbad, CA) and gene expression was induced by addition of 100 ng/ml doxycycline (Sigma, St. Louis, Missouri, United States) for 12-24 hr. *E. coli* BL21 (DH5a) (ThermoFisher Scientific, Waltham, Massachusetts, United States), BL21(DE3)-RIL and BL21CodonPlus(DE3)-RIL (Agilent Technologies, Santa Clara, California, United States) strains were cultured on LB agar or liquid media at 37°C. LB supplemented with ampicillin (50 μg/ml) to maintain the pETDuet plasmids and with chloramphenicol (34 μg/ml) to maintain the extra copies of tRNA Genes in CodonPlus strain. SF9 (ThermoFisher Scientific, Waltham, Massachusetts, United States) and Tnao38 (gift from Garry W Blissard) cells were maintain in Sf-900 II medium (ThermoFisher Scientific, Waltham, Massachusetts, United States) supplemented with 10% (v/v) fetal bovine serum, at 27°C and 110 rpm orbital rotation.

## METHOD DETAILS

### Cell transfection and electroporation

CENP-B-INCENP-EGFP gene expression was induced by addition of 10 ng/ml doxycycline (Sigma, St. Louis, Missouri, United States) for 12-24 hours. To achieve single depletion of either Bub1 or CENP-Q, cells were transfected with either Lipofectamine 2000 or RNAiMAX(Invitrogen, Carlsbad, California, United States) and Bub1 siRNA (Dharmacon, part of GE Healthcare, Piscataway, NJ; 5′-GUUGCCAACACAAGUUCU-3′) or CENP-Q siRNA (CENP-Q (GAGUUAAUGACUGGGAAUA; AUGGAAAGGGCACGAAGACA; ACAAAGCACACUAACCUAA; UGUCAGAGAAUAAGGUUAG;) at 50 nM for respectively 24 and 48 hours using manufacturer's protocol. Depletion of endogenous CENP-OQU was achieved with two rounds of Lipofectamine RNAiMAX transfection, for a total of 72 hours, with the following siRNA oligos at a total concentration of 100 nM: CENP-Q (GAGUUAAUGACUGGGAAUA; AUGGAAAGGGCACGAAGACA; ACAAAGCACACUAACCUAA; UGUCAGAGAAUAAGGUUAG; GGUCUGGCAUUACUACAGGAAGAAA), CENP-U: (GAAAGCCAUCUGCGAAAUA; GAAAAUAAGUACACAACGU; GGGAAGAUAUCUCAUGACA; GCGCAAGACGUUCAAAGAA) and CENP-O (GUACGAAGCCCUUGCAUCA; AAGCCAUUCUGCAGGCAUA; GCUCACACAAUCCACGAACA; CUAGAUUGCUGUAUAAGGA). For rescue experiments, 48 hours into the siRNA depletion of endogenous OQU, we performed electroporation of Alexa488 labeled recombinant CENP-OPQUR at a concentration of 4 μM as previously described (Alex et al., 2019; Pesenti et al.,

2018)(Neon Transfection System, Thermo Fisher). As control we used Alexa488. Following recovery from electroporation, cells were arrested in mitosis with a 3.3 μm nocodazole (Sigma-Aldrich, Missouri, USA) treatment for 16 hours and then prepared for immunofluorescence analysis. For co-depletion of endogenous OQU with either Bub1 or BubR1, cells were treated with 100 nM of siBUB1 or siBUBR1 RNA duplexes as previously described (Overlack et al., 2015) for the last 24 hours of the experiment, where 4 hours before fixation cells were treated with 3.3 μM nocodazole followed by 2 hours treatment with 100 nM Okadaic acid. U2OS-lacO cells were transfected with the LacI-EGFP-CENP-U full length or deletion/mutant constructs using X-tremeGENE (Roche, Basel, Switzerland) transfection reagent (3:1 ratio) for 48 hours using manufacturer's protocol.

## Plasmids

To generate plasmids for expressing N terminus tagged Lac-I-EGFP-CENP-U full length or deletion proteins in U2OS-lacO cells, CENP-U gene was PCR amplified from the codon optimized CENP-U cDNA (GeneArt, Life Technologies, Carlsbad, California, United States) and cloned into the pCDNA5/FRT/TO-EGFP-IRES (Petrovic et al., 2010), a modified form of pCDNA5/FRT/TO vector (Invitrogen, Carlsbad, California, United States)) between the BamHI and *Xho*I restriction sites. LacI gene was PCR-amplified and inserted in the same reading frame between the *Pme*I restriction sites using the Gibson cloning compatible primers. To generate a plasmid for expressing CENP-B (2-164)-INCENP (48-918)-EGFP, the gene sequences were sub-cloned from the SL417 vector (Liu et al., 2009) into pCDNA5/FRT/TO-EGFP-IRES between BamHI and *Not*I restriction sites (De Antoni et al., 2012). To generate a plasmid for expressing N terminus 6xHis tagged PLK1 recombinant protein in insect cells, codon optimized PLK1 cDNA (GeneArt, Life Technologies) was sub-cloned between the BamHI and SalI restriction sites of a modified pLIB (Clontech, now TAKARA Bio USA, Kyoto, Kyoto, Japan) vector already containing 6xHis followed by TEV protease sequences (as described in Pan et al. [2017]). Plasmids to express 6xHis-MBP-PBD and 6xHis-MBP-PLK1$^{T210A}$ in bacterial cells were generated by cloning the PCR amplified sequences for the polo-box-domain (PBD; amino acids 345-603) of PLK1 and full length PLK1 (T210 residue was mutated to alanine using site-directed mutagenesis), respectively, between the BamHI and SalI restriction sites of a modified pETDuet-1 (Novagen) vector, already containing 6xHis followed by PreScission Protease-MBP-TEV protease sequences. HsMPS1 was PCR-amplified from a human cDNA library and sub-cloned in a modified pLIB vector in frame with the sequence encoding GST and a PreScission protease cleavage site. Plasmids to express N terminus tagged GST-CDK1 and 6xHis tagged Cyclin B1 were generated by sub-cloning, codon optimized cDNA of CDK1 and Cyclin B1 (GeneArt, Life Technologies) between the BamHI and SalI restriction sites of a modified pLIB vectors containing sequences for the GST followed by PreScission protease and 6xHis followed by TEV protease, respectively. These pLIB plasmids generated so-forth were used to insert the GST-CDK1 and His-Cyclin B1 sequences into a baculovirus-based multigene-expressing vector, pBIGa (Weissmann et al., 2016) by Gibson cloning method. CENP-OP and CENP-QU plasmids were published previously (Pesenti et al., 2018). To generate plasmids for expressing CENP-OPQUR and CENP-OPQU$^{\Delta1\text{-}114}$R complexes in insect cells, plasmid to express N terminus 6xHis tagged CENP-Q were generated by Gibson cloning method, codon optimized cDNA of CENP-Q (GeneArt, Life Technologies) was inserted in a modified pLIB vectors containing sequences for the 6xHis followed by TEV protease. The codon optimized cDNA of CENP-O, -P, -U- U$^{\Delta1\text{-}114}$, and -R were inserted by Gibson cloning method in to unmodified pLIB plasmids. These pLIB plasmids generated so-forth were used to insert the CENP-O, -P, -U, -U$^{\Delta1\text{-}114}$, -R and 6His-CENP-Q sequences into two baculovirus-based multigene-expressing vectors, pBIGa (Weissmann et al., 2016) by Gibson assembly, one containing CENP-O, -P, -U, -R and −6His-CENP-Q, and one containing CENP-O, -P, -U$^{\Delta1\text{-}114}$, -R and 6His-CENP-Q. CENP-LN, CENP-C$^{1\text{-}544}$HKI$^{57\text{-}C}$M, Mis12, NDC80, KNL1, BUB1:BUB3, and BUBR1:BUB3 complexes were previously published (Breit et al., 2015; Huis In 't Veld et al., 2016; Klare et al., 2015; Pentakota et al., 2017; Petrovic et al., 2014). Plasmids to express 6xHis-MBP-CENP-U$^{58\text{-}114}$ wild-type, S77A/T78A and T98A, in bacterial cells were generated by cloning the PCR amplified sequences for CENP-U$^{58\text{-}114}$ (amino acids 58-114) of codon-optimized CENP-U cDNA, between the BamHI and *Hind*III restriction sites of a modified pETDuet-1 (Novagen) vector, already containing 6xHis followed by PreScission Protease-MBP-TEV protease sequences. The MBP-CENP-U$^{58\text{-}114}$S77A/T78A and T98A mutants were generated by mutating S77/T78 and T98 residues in alanine using site-directed mutagenesis.

## Cell synchronization

To test the effect of various kinases and phosphatases on the localization of kinetochore proteins cells were synchronized using double thymidine arrest. Cells were released from 18 hours thymidine (2 mM; Sigma–Aldrich) block by washing them with the fresh media several times. After releasing them for the next 9 hours, second exposure to thymidine (2 mM) was continued for another 15 hours. Cells were released into the S phase for 4 hours and then nocodazole (3.3 μM) was added to the media for the next 3-4 hours to enrich the mitotic cell population. Kinase activity inhibitors, RO-3306 (9 μM), BI 2536 (100 nM), hesperadin (500 nM), reversine (500 nM)(Calbiochem) and/or phosphatase inhibitor, okadaic acid (100 nM; Calbiochem) were added in presence of MG132 proteasome inhibitor (10 μM; Calbiochem) to the cells for 10, 30, or 90 minutes before fixing for immunofluorescence or harvesting for western blotting analysis. H3-pS10 staining was used to indicate the potency of hesperadin directly and RO-3306 indirectly, whereas, Cep135, a centrosome marker was used to indicate the absence of PLK1 from centrosome as well, when BI-2536 was used, thus indicating its potency. CREST was used as kinetochore marker and DAPI indicates mitotic cells.

## Immunofluorescence

Cells were grown on coverslips pre-coated with 0.01% poly-D-lysine (Sigma-Aldrich). Cells were pre-permealized with 0.5% Triton X-100 solution in PHEM (Pipes, HEPES, EGTA, $MgCl_2$) buffer for 2-5 minutes before fixing with 4% PFA in PHEM for 15-20 minutes.

After blocking the cells with either 3% BSAor 5% boiled goat serum in PHEM buffer supplemented with 0.1% Triton X-100 (PHEM-T), they were incubated at room temperature for 1-2 or 16 hours at 4°C with the following primary antibodies: anti-CENP-QU (in-house generated; goat 1:100), anti CENP-O (rabbit; 1:500) (Amaro et al., 2010), anti-PLK1 (Abcam #ab17057, mouse monoclonal antibody; 1:300), anti-H3-pS10 (Abcam # ab5176, rabbit polyclonal antibody, 1:2000), rabbit anti-CEP135 (gift from Alex Bird [Bird and Hyman, 2008], 1:3000), anti-BUB1 (Abcam #ab9000, rabbit polyclonal antibody, 1:1000), anti-BubR1 (rabbit polyclonal, Abcam, ab70544, 1:500), anti-Aurora B (mouse monoclonal, Abcam, ab3609, 1:500), anti-Mps1 (rabbit polyclonal affinity purified, #933, produced in house, 1:500), anti-AurB-pT232 (Rockland #660-401-667, rabbit polyclonal antibody, 1:2000), anti-H2ApT120 (Active Motif #39391, rabbit polyclonal antibody, 1:2000), CREST/anticentromere antibody (human autoimmune serum, Antibodies, Inc., 1:100) diluted in the blocking buffer. Washings were done in PHEM-T buffer. Donkey anti-rabbit Alexa Fluor 488 (Invitrogn A21206), Goat anti-rabbit DyLight 405 (Jackson Immuno Research 111-475-003), Donkey anti-goat 488 (Invitrogen, Carlsbad, California, United States), Goat anti-human Alexa Fluor 647 (Invitrogen, Carlsbad, California, United States), Chicken anti-rabbit Alexa Fluor 647 (Invitrogen, Carlsbad, California, United States A11046) and goat anti-mouse Rhodamine Red (Jackson Immuno Research) were used as secondary antibodies. DNA was stained with 0.5 μg/ml DAPI (Serva) and Mowiol (Calbiochem) was used as mounting media.

### Western blotting

Cell pellets were resuspended in sample buffer, boiled and analyzed by western blotting. Membranes were probed with the following antibodies: anti-GFP (rabbit polyclonal, Abcam, ab190584, 1:10000), anti-Bub1 (rabbit polyclonal; Abcam, Cambridge, UK; 1:5000), anti-BubR1 (mouse monoclonal; BD #612503, 1:1000) and anti-Tubulin (mouse monoclonal; Sigma; 1:8000), anti-Incenp (rabbit polyclonal, Cell Signaling #2807, 1:500), anti-Cyclin B (mouse monoclonal, Santa Cruz, sc-245, 1:1000), anti-PLK1 (mouse monoclonal; Abcam #ab17057, 1:1000), anti-Vinculin (mouse monoclonal, Sigma, V9131, 1:10000).

### Cell imaging

Cells were imaged at room temperature using a spinning disk confocal device on the 3i Marianas system equipped with an Axio Observer Z1 microscope (Zeiss), a CSU-X1 confocal scanner unit (Yokogawa Electric Corporation, Tokyo, Japan), 100 × /1.4NA Oil Objectives (Zeiss), and Orca Flash 4.0 sCMOS Camera (Hamamatsu). Images were acquired as z sections at 0.25 μm. Images were converted into maximal intensity projections, exported, and converted into 8-bit using ImageJ. Images were cropped and merged in ImageJ. The figures were arranged using Adobe Illustrator software. either Imaris 7.3.4 and 9.2 software (Bitplane, Zurich, Switzerland) or with ImageJ/Fiji (Schindelin et al., 2012).

### Protein expression and purification

6xHis-PLK1, GST-CDK1/Cyclin B1 complex, and GST-MPS1 were expressed in insect cells. High-titer virus (V2) produced in Sf9 cells was used to express protein in Tnao38 insect cells (72 hours, 27°C). 6xHis-MBP-PBD and 6xHis-MBP-PLK1$^{T210A}$ were expressed in *E. coli* BL21 (DE3) cells using 0.2 mM IPTG for approximately 15 hours at 18°C. To purify 6xHis-PLK1, 6xHis-MBP-PBD or 6xHis-MBP-PLK1$^{T210A}$, cells were pelleted down and re-suspended in His-lysis buffer (50 mM HEPES pH 7.5, 500 mM NaCl, 5% (v/v) Glycerol, 10 mM Imidazole and 2 mM TCEP) supplemented with protease inhibitor cocktail (Serva). In case of GST-Cdk1/His-Cyclin B1 complex, cell pellet was re-suspended in GST-lysis buffer (50 mM HEPES pH 7.5, 300 mM NaCl, 5% (v/v) Glycerol, 2 mM TCEP) and in case of GST-MPS1 in GST-lysis buffer (50 mM HEPES pH 7.5, 500 mM NaCl, 5% (v/v) glycerol, 1 mM TCEP). After sonication, cell suspension was clarified and applied to a pre-equilibrated, 5 mL HisTALON Cartridge pre-packed TALON Superflow Resin (Clontech) or Glutathione Sepharose 4 Fast Flow beads (GE Healthcare), respectively. Column or beads were washed with at least 10 volumes of respective lysis buffer and protein was eluted using either His-lysis buffer supplemented with 250 mM imidazole or GST-lysis buffer supplemented with 20 mM reduced Glutathione, respectively. Protein fractions were pooled and concentrated in order to load on a Superdex 200 16/60 size exclusion chromatography (SEC) column, pre-equilibrated with SEC buffer (20 mM HEPES pH 7.5, 200 mM NaCl, 5% (v/v) Glycerol and 1 mM TCEP), and in case of GST-MPS1 with SEC buffer (25 mM HEPES pH 7.5, 150 mM NaCl, 5% (v/v) glycerol, 1 mM TCEP). Fractions containing protein of interest, as analyzed by 12.5% SDS-PAGE, were pooled, concentrated, flash frozen in liquid nitrogen and stored at – 80°C. CENP-OPQUR, CENP-QU and CENP-OP has been purified as described previously (Pesenti et al., 2018). CENP-OPQU$^{\Delta 1\text{-}114}$R was purified using the previously described protocol for CENP-OPQUR wild-type (Pesenti et al., 2018). *Escherichia coli* BL21 (DE3) cells harboring vectors expressing 6His-MBP-CENP-U58-114 wt and mutants were grown in Terrific Broth at 37°C to an OD600 of 0.6 - 0.8, when 0.2 mM IPTG was added and the culture was grown at 18°C for ~15 hours. Cell pellets were resuspended in lysis buffer (20 mM Tris/HCl pH 6.8, 300 mM NaCl, 7 mM imidazole, 5% (v/v) glycerol and 1 mM TCEP) supplemented with protease inhibitor cocktail, lysed by sonication and cleared by centrifugation at 108,000 g at 4°C for 1 hour. The cleared lysate was applied to 5 mL HisTALON Cartridges pre-packed with TALON Superflow Resin (Clontech) pre-equilibrated in lysis buffer, washed with 10 volumes of lysis buffer. Bound proteins were eluted with lysis buffer supplemented with 250 mM imidazole. The fractions containing the 6His-MBP-CENP-$^{U58\text{-}114}$wt and mutants were then diluted in 10 volumes of 20 mM Tris/HCl pH 6.8, 5% glycerol, 1 mM TCEP. Resource Q anion exchange chromatography column (GE Healthcare) was pre-equilibrated in 20 mM Tris/HCl pH 6.8, 30 mM NaCl, 5% (v/v) glycerol, 1 mM TCEP. The sample now adjusted to a salt concentration of 30 mM was loaded onto the Resource Q column and eluted with a linear gradient of 30 - 1000 mM NaCl in 15 bed column volumes. Fractions containing 6His-MBP-CENP-$^{U58\text{-}114}$wt and mutants complex were pooled and concentrated and loaded onto a Superdex 75 16/60 SEC column (GE Healthcare) pre-equilibrated in SEC buffer (20 mM Tris pH 6.8, 300 mM NaCl,

5% (v/v) glycerol and 1 mM TCEP). Fractions containing 6His-MBP-CENP-$^{U58-114}$wt and mutants were concentrated, flash-frozen in liquid nitrogen and stored at −80°C. CENP-LN, CENP-C$^{1-544}$HKI$^{57-C}$M, Mis12, NDC80, KNL1, BUB1:BUB3 and BUBR1:BUB3 complexes, BUB1 kinase (BUB1$^{705-1050}$) and Aurora B kinase (Aurora B$^{45-344}$:INCENP$^{835-903}$) were expressed and purified according to previously published protocols (Breit et al., 2015; Huis In 't Veld et al., 2016; Klare et al., 2015; Pentakota et al., 2017; Petrovic et al., 2014; Sessa et al., 2005)

### *In vitro* assembly of rKT and rKT containing CENP-U$^{\Delta 1-114}$

Reconstitution of rKT and rKT containing CENP-U$^{\Delta 1-114}$ particles was performed as previously published in Pesenti et al., 2018. In brief, a stoichiometric amount of purified CENP-LN, CENP-CHKIM, CENP-OPQUR, Mis12, Ndc80 and KNL1 complexes were incubated at 4°C for minimum 1 hour and purified by SEC using a buffer containing 20 mM Tris pH 6.8, 300 mM NaCl, 5% (v/v) glycerol and 1 mM TCEP.

### Recombinant proteins fluorescence labeling

MBP-PLK1$^{PBD}$, MBP-PLK1$^{201A}$, CENP-OPQUR and CENP-OPQU$^{\Delta 1-114}$R were labeled using Alexa Fluor 488 Protein Labeling Kit (ThermoFisher Scientific, Waltham, Massachusetts, United States) according to the manufacturer instructions.

### *In vitro* phosphorylation of rKT, rKT containing CENP-U$^{\Delta 1-114}$, CENP-OPQUR, -OPQU$^{\Delta 1-114}$R, -OP, -QU, 6His-MBP-CENP-U$^{58-114}$-WT and mutants, BUB1:BUB3 and BUBR1:BUB3

CENP-OPQUR, -OPQU$^{\Delta 1-114}$R, CENP-QU and CENP-OP purified from insect cell were carefully de-phosphorylated by treatment with lambda phosphatase (produced in house) as described previously (Pesenti et al., 2018). The phosphorylation of these recombinant proteins was performed in SEC buffer supplemented by 2 mM of ATP and 10 mM of $MgCl_2$. A ratio kinase/protein of 1/25 for CDK1 (in house production), Aurora B (in house production), MPS1 (in house production) and BUB1 (in house production), and 1/20 to 1/10 for PLK1 (in house production) depending of the activity of the recombinant kinase. If the proteins used in the reaction were previously treated with lambda phosphatase 1mM of sodium orthovanadate and 5μM of okadaic acid were added to the reaction. The reactions were incubated at 4 or 10°C for 16h and submitted to analyze by mass spectrometry and phosphostaining.

### Phosphostaining of recombinant proteins

Samples containing equal amount of un-phosphorylated and phosphorylated proteins were separated by 12.5% SDS-PAGE and stained by Pro-Q Diamond phosphoprotein stain (Invitrogen, Carlsbad, California, United States) according to the manufacturer instruction. Images were acquired using a BioRAD chemiDoc MP Imaging System (BioRAD). Images were adjusted using Image Lab software Version 5.2 (BioRAD). The same gel was subsequently stained with Coomassie stain.

### Analytical SEC

Analytical size exclusion chromatography was carried out on a Superdex 200 5/150 or Superose 6 5/150 in a buffer containing 20 mM Tris or HEPES pH 6.8, 300 mM NaCl, 2,5% (v/v) glycerol and 1 mM TCEP on an ÄKTA micro system. All samples were eluted under isocratic conditions at 4°C in SEC buffer (20 mM Tris or HEPES pH 6.8, 300 mM NaCl, 5% (v/v) glycerol and 1 mM TCEP) at a flow rate of 0.15 ml/min. Elution of proteins was monitored at 280 nm and 488 nm in case of MBP-PLK1$^{210A}$ and MBP-PLK1$^{PBD}$ labeled with Alexa488. 100 μL fractions were collected and analyzed by SDS-PAGE and Coomassie blue staining. In experiments were MBP-PLK1$^{210A}$ and MBP-PLK1$^{PBD}$ labeled with Alexa488 were used, the in-gel detection of the fluorescence was detected using a BioRAD chemiDoc MP Imaging System (BioRAD). To detect the formation of a complex, proteins were mixed at the concentrations of 5 μM in 50 μl, incubated for at least 1 hour on ice, subjected to SEC then analyzed by SDS-PAGE.

### Analytical ultracentrifugation (AUC)

Sedimentation velocity experiments were performed in an Optima XL-A analytical ultracentrifuge (Beckman Coulter, Palo Alto, US-CA) with Epon charcoal-filled double-sector quartz cells and an An-60 Ti rotor (Beckman Coulter, Palo Alto, US-CA). Samples were centrifuged at 203,000xg at 20°C and 500 radial absorbance scans at 488 nm and collected with a time interval of 1 min. Analysis of MBP-PLK1$^{210A}$ and MBP-PLK1$^{210A}$:CENP-OPQUR complex were carried out at 20°C in 20 mM HEPES pH 7.5, 2.5% (v/v) glycerol, 300 mM NaCl and 1 mM TCEP.

### Mass spectrometry and phosphorylation site analysis

Liquid chromatography coupled with mass spectrometry was used to assess the phosphorylation status of CenpU. CENP-QU or CENP-OPQUR FL were *in vitro* phosphorylated by CDK1 or PLK1 alone or in combination. Mutants (S77A/T78A or 98A) were phosphorylated in the context of MBP-CENP-U$^{58-114}$. Controls by omitting the kinase(s) were performed for all samples. Samples were reduced, alkylated and digested with LysC/Trypsin and prepared for mass spectrometry as previously described (Rappsilber et al., 2007). 100 ng of obtained peptides were separated on a ThermoFisher Scientific EASY-nLC 1000 HPLC system (ThermoFisher Scientific, Waltham, Massachusetts, United States) using an 45 min gradient from 5%–60% acetonitrile with 0.1% formic acid and directly sprayed via a nano-electrospray source in a Q Exactive (ThermoFisher Scientific, Waltham, Massachusetts, United States)

(Michalski et al., 2011). The Q Exactive was operated in data-dependent mode acquiring one survey scan and subsequently ten MS/MS scans (Olsen et al., 2007). Samples were measured at least three times.

## QUANTIFICATION AND STATISTICAL ANALYSIS

### Cell image analysis

For Imaris quantifications, CREST signal was used as reference channel and spots were placed on kinetochores using automatic setting in Imaris. Four spots of same size were placed manually in cytoplasm and their average was used as background for respective channel. After background subtraction, ratio of intensity mean signal of the protein of interest versus CREST was used to plot the graphs. In case of U2OS lacO-lacI experiments, GFP channel was used as a reference channel to put a surface manually on ectopic foci. A spot was placed manually in the cytoplasm and the value was used as background for respective channel. After background subtraction, intensity mean of PLK1 versus GFP was used to plot the graphs. ImageJ/Fiji quantifications were performed using a semi-automated script (Pan et al., 2017). Intensity measurements were exported to Excel (Microsoft) and graphs were plotted using Prism software. Sample size is indicated for each figure. Statistical analysis was performed with a rank sum, nonparametric test comparing two unpaired groups (Mann-Whitney test). Symbols indicates: n.s = $p > 0.05$, * = $p \leq 0.05$, ** = $p \leq 0.01$, *** = $p \leq 0.001$, **** = $p \leq 0.0001$.

### AUC analysis

Data was analyzed using the SEDFIT software (Schuck, 2000) in terms of continuous distribution function of sedimentation coefficients (c(S)). The protein partial specific volume was estimated from the amino acid sequence using the program SEDNTERP. Data were plotted using the program GUSSI, which is freely available from https://www.utsouthwestern.edu/labs/mbr/software/. The calculated values for the buffer density and the viscosity are 1.01928 g/ml and 1.1190 cP respectively. The calculated values of the partial specific volume [V(bar), inverse of density] at 20°C for MBP-PLK1$^{210A}$ is 0.7424 ml/g and for MBP-PLK1$^{210A}$:CENP-OP-QUR complex is 0.7404 ml/g.

### Mass Spectrometry analysis

Mass spectrometry raw files were processed with the MaxQuant software (version 1.5.2.18) using a reduced database containing only the proteins present in the samples for the search giving deamidation (NQ), oxidation (M) and phosphorylation (STY) as variable modifications and carbamidomethylation (C) as fixed modification (Cox and Mann, 2008). A false discovery rate cut-off of 1% was applied at the peptide and protein levels and as well on the phosphorylation site table (Cox and Mann, 2008). Identified phosphorylation sites were further analyzed for their localization probability and only unambiguous identified sites were kept. MS/MS spectra were additionally manually inspected. Peptide peaks and isotope patterns from MS scans containing Thr78 or Thr98 were directly extracted from Xcalibur (ThermoFisher Scientific, Waltham, Massachusetts, United States).